Four-wave-mixing processes in translational optomechanical media

D. Rogovin, T. P. Shen, and J. Scholl
Rockwell Science Center, Thousand Oaks, California 91360
(Received 23 January 1992; revised manuscript received 6 July 1992)

We study the mechanical, dielectric, and nonlinear-optical response of translational optomechanical media to incident electromagnetic radiation. These media consist of three-dimensional arrays of electrically small, isotropic particles that are mechanically supported but free to roll on stacks of very thin transparent planes. Electrostrictive forces tend to move the spheres in such a way as to form spatial variations in the particle density that correspond to electromagnetically induced spatial modulations in the array's dielectric constant. These modulations constitute translational optical index gratings that can be used to control the propagation characteristics of electromagnetic radiation. We study optical phase conjugation, pump-beam modulation, and harmonic phase conjugation at submillimeter, millimeter, and microwave wavelengths in this class of nonlinear media. We also examine the dynamics of these media from the perspective of the Langevin equations and determine the influence of thermal fluctuations on the properties of such an array.

PACS number(s): 42.65.Hw

I. INTRODUCTION

In an extensive series of experimental studies Ashkin *et al.* [1–4] examined the nonlinear-optical properties of liquid suspensions of submicrometer-sized polystyrene spheres. The basic mechanism for nonlinear-optical behavior in these liquid suspensions is based on electrostrictive forces that give rise to static density variations in the particle density that set up spatial modulations in the suspension's optical index of refraction. These spatial modulations constitute translational index gratings that can be used to control the propagation characteristics of incident electromagnetic radiation. In particular, self-focusing [2], optical bistability [4] and optical phase conjugation [1] were successfully demonstrated in this interesting class of nonlinear media. These studies were conducted at visible wavelengths and it is of interest to examine the possibility of extending such research to longer wavelengths.

The observed nonlinear-optical characteristics of liquid suspensions of microspheres are characterized by their very large third-order susceptibilities. Typically these are on the order of 10^{-9} cm^2/W for 1000-Å spheres and scale with the particle volume for a constant volume fraction of microparticles. Accordingly, for active millimeter wave optics it should be possible to scale the particle size up to tens of micrometers without suffering significant scattering losses. For these size particles we anticipate that the third-order optical susceptibility should scale to 10^{-3} cm^2/W or more.

We can most readily appreciate the need for novel materials in this spectral region by contrasting phase conjugation at 0.5 μm and 1 mm wavelengths for standard Kerr media. Specifically, Table I contrasts the efficiency, ξ ($\xi=\tan^2\kappa L$, with $\kappa=4\pi\chi^{(3)}I_{\text{pump}}/\lambda$, with L the optical pathlength and I_{pump} the pump intensity) for generating phase conjugate radiation at these two wavelengths. An examination of Table I reveals that it is extremely difficult to extend four-wave-mixing processes to such long wavelengths due to the problems associated with beam intensities and the scaling properties of the nonlinear susceptibilities. For example, due to diffraction, incident radiation cannot be focused down to distances less than the wavelength λ. Since laboratory cw power sources at millimeter wave and visible wavelengths are of the same order of magnitude, it follows that the four-wave-mixing coefficient κ, which is proportional to the I_{pump}/λ, will scale as λ^{-3}. Thus κL declines by some nine orders of magnitude if one attempts to scale from visible to millimeter wavelengths, unless materials with unusually large nonlinear-optical susceptibilities are available.

The discussion above clearly indicates that artificial Kerr media would be very interesting candidates for nonlinear-optical processes at long wavelengths due to their large nonlinear susceptibilities. However, the dynamics of liquid suspension of microspheres are dominated by diffusion in a viscous fluid [5] and the dielectric response times of these media are quite slow. Typical response times for 1000-Å particles irradiated by argon-ion light are on the order of a second and these times scale with the square of the radiation wavelength λ. For millimeter wavelengths the medium response time scales to more than 10^4 sec, which is too long for feasible labo-

TABLE I. Difficulties at long wavelengths.

Physical parameter	Visible wavelengths	Millimeter wavelengths
Wavelength	0.5 μm	1 mm
Pump intensity	10^8 W/cm^2	25 W/cm^2
Typical values of $\chi^{(3)}$	10^{-10} esu	10^{-10} esu
Optical pathlength	2 mm	30 cm
κL	1.2	10^{-8}
Efficiency	gain	negligible

ratory experiments. Thus, use of particle translation as a means to achieve nonlinear-optical processes from submillimeter wave to microwave wavelengths requires significant improvement of the medium response time to be of any interest [6].

In suspensions, the fluid supports the spheres and acts as a source of dissipation so that the medium can achieve steady state. However, it does this at the expense of mechanical stability (in the sense that the microparticles are subject to coagulation or sedimentation) and long optical response times. Furthermore, only fluids that are nonabsorbent at the wavelengths of interest can be used as the host. This raises additional constraints for using suspensions as active media in nonlinear electromagnetic processes for device applications at long wavelengths.

It is tempting to consider the possibility of nonlinear media that are based on the same physical principles as suspensions, but are not subject to the limitations that are imposed on the medium by the presence of a viscous fluid. For example, Palmer [7–8] has conjectured that aerosols might be useful active media for nonlinear processes. However, aerosols are volume fraction limited and are often difficult to maintain over extended periods of time.

In this paper we examine the optical properties of a new class of artificial dielectric media consisting of three-dimensional arrays of electrically small, isotropic spheres that are mechanically supported but free to roll [9]. The spheres are supported on stacks of flat, very thin (much less than the radiation wavelength) transparent planes. The array is maintained in air, whose viscosity enables the system to achieve a steady state. We shall refer to such arrays as translational optomechanical media and demonstrate that they have unique nonlinear-optical and dynamical properties. In addition, such arrays enjoy a number of practical advantages over suspensions for device applications: specifically, stability against coagulation or precipitation, fast optical response times, as well as overall thermal, optical, and mechanical stability and control.

The dynamical characteristics of such an array are different from those of liquid suspensions. For example, the much smaller viscosity coefficient of air, relative to common liquids such as water, implies that the medium response time for corresponding wavelengths will be much shorter than that of a suspension. Furthermore, the greater size of the particles implies larger particle polarizabilities and much stronger electrostrictive forces. This ensures that the array will operate in the driven and not the diffusive regime, even at low beam intensities, and further reduces the medium's dielectric response time.

In the overdamped state an array can be described by the Planck-Nernst equation, which also dictates suspension [5] dynamics. However, we find that, unlike a suspension whose dynamics are always governed by diffusion, it is possible for a translational optomechanical medium to achieve underdamped states where its dielectric response to incident radiation displays oscillations as it evolves towards steady state.

Scattering losses require that the sphere radius $r_0 \ll \lambda$, and since the unsaturated nonlinear optical susceptibilities scale as r_0^3 (for a fixed particle volume fraction), it is natural to consider active optical processes at long wavelengths. In particular, the fabrication of small metallic, metal coated, or dielectric spheres, on a size scale of $1-100\ \mu$m or more is quite feasible. This implies that optomechanical media are most applicable to active optical processes for electromagnetic wavelengths on the order of several hundred μm to several cm. Thus, our interest focuses on the spectral range spanning the submillimeter to the microwave region of the electromagnetic spectrum. Longer wavelengths are possible; however, they require construction of very large three-dimensional arrays of particles, on the order of tens of m. Although it is quite possible to fabricate such devices, they are too large for convenient laboratory studies and will not be discussed here.

This paper, which deals with the mechanical, dielectric, and nonlinear-optical response of these three-dimensional arrays to electromagnetic radiation, is divided into six sections. In Sec. II we discuss the interaction of electromagnetic radiation with translational, optomechanical media. We determine the equilibrium particle density and nonlinear-optical susceptibilities versus radiation power and array parameters for a translational optomechanical medium irradiated by two degenerate, plane-wave cw beams that form a coherent, static electromagnetic grating. Section III deals with the transient dynamics of rolling spheres. We investigate the dynamics of small spheres that are free to roll on flat, transparent, very thin planes from the perspective of the Langevin equations. We examine the response of a sphere to a static index grating created by two coherently interfering degenerate, cw plane-wave beams. We also study the role of Brownian fluctuations, arising from collisions of these spheres with air molecules, in grating dynamics. In Sec. IV, we utilize a Monte Carlo calculation to investigate the transient dynamics of an ensemble of spherical particles subject to a static electromagnetic grating in the presence of thermal noise. We also examine array dynamics from the perspective of the Planck-Nernst equation and obtain the same transient dynamics for the overdamped case as the Monte Carlo calculation. In Sec. V, we study optical phase conjugation, pump grating modulation [10], and harmonic phase conjugation [11] at long wavelengths. We summarize this work in Sec. VI. In following studies we will examine other optomechanical media, such as arrays of anisotropic particles which form orientational gratings [12].

II. INTERACTION OF ELECTROMAGNETIC RADIATION WITH TRANSLATIONAL OPTOMECHANICAL MEDIA

In Sec. II A we develop a theory that describes the interaction of electromagnetic radiation with three-dimensional arrays of translational optomechanical media. In Sec. II B the effective third-order susceptibility is calculated for the case of a single beam, and in Sec. II C we examine the response of this optomechanical medium to two degenerate, plane-wave cw beams.

A. Steady-state density and nonlinear polarization

Our interest focuses on small dielectric, metallic, or metal-coated spheres that are supported on stacks of flat, very thin, transparent planes, oriented perpendicular to gravity. There are three forces: (i) the electrostrictive force that tends to move the spheres, (ii) friction which tends to retard all motion, and (iii) the reaction forces associated with the constraints imposed on particle dynamics.

The motion induced by the electrostrictive force [5] will change the sphere density. The altered particle density implies a spatially varying dielectric constant whose characteristics depend upon the field intensities and wave vectors. The presence of friction insures energy dissipation and the eventual attainment of statistical equilibrium. Finally, the reaction forces associated with the constraints alter the friction coefficients between the spheres and their support structures.

In the presence of a radiation field $\mathbf{E}(\mathbf{r},t)$, each sphere acquires an induced electric dipole moment $\mathbf{p}(\mathbf{r},t)$ given by

$$\mathbf{p}(\mathbf{r},t)=\alpha\mathbf{E}(\mathbf{r},t) , \tag{2.1}$$

where α is the polarizability of a given sphere. If the sphere is composed of a dielectric material, its radius $r_0 \ll \lambda$ and the host air, then α is given by

$$\alpha=\frac{\epsilon_B-1}{\epsilon_B+2}r_0^3 , \tag{2.2}$$

where ϵ_B is the sphere's dielectric constant. For a metallic or metal-coated sphere (the coating thickness is greater than the penetration depth) and wavelengths greater than several hundred μm, $\epsilon_B \to -\infty$ and $\alpha \to r_0^3$. The induced dipole moment couples back to $\mathbf{E}(\mathbf{r},t)$ to generate an electrostrictive potential $U(\mathbf{r})$:

$$U(\mathbf{r})=-\tfrac{1}{2}\overline{\mathbf{p}(\mathbf{r},\mathbf{t})\cdot\mathbf{E}(\mathbf{r},\mathbf{t})}=-\tfrac{1}{2}\alpha\overline{\mathbf{E}^2(\mathbf{r},\mathbf{t})} . \tag{2.3}$$

Here the overbar implies an average over a time long compared to an optical period, but short compared to the medium response time. Associated with $U(\mathbf{r})$ is an electrostrictive force $\mathbf{F}(\mathbf{r})=-\nabla U(\mathbf{r})$ that is largest for metallic or metal-coated spheres.

The spheres are confined to the surface of the planes $z=z_m$, so that they cannot move freely in the z direction, which notably complicates analysis. To simplify matters, we will assume that the incident beams are all polarized parallel to these planes. It is worth noting that the presence of these planes induces an anisotropy in the optomechanical medium's response to radiation. In particular, the spheres will not respond if the incident beam is polarized perpendicular to the support planes.

The presence of dissipation through friction with air and contact with the mechanical support structures ensures that we may use statistical mechanics to determine the sphere density, provided the particles do not get stuck due to static friction. If this does not occur, the equilibrium sphere density is specified by the Maxwell-Boltzmann distribution

$$n(\mathbf{r})=n_0\frac{\exp\left[-\dfrac{U(\mathbf{r})}{kT}\right]}{\dfrac{1}{V}\int d^3r\exp\left[-\dfrac{U(\mathbf{r})}{kT}\right]} , \tag{2.4}$$

where n_0 is the unperturbed sphere density, V is the interaction volume, and Eq. (2.4) assumes that $\mathbf{r}$ in the plane of the spheres. If $\mathbf{r}$ is off the planes,

$$n(\mathbf{r})=N_\Sigma\frac{\displaystyle\sum_{m=1}^{N_z}\delta(z-z_m)\exp\left[-\frac{U(\mathbf{r})}{kT}\right]}{\displaystyle\int_0^L dx\int_0^L dy\int_0^L dz\sum_{m=1}^{N_z}\delta(z-z_m)\exp\left[-\frac{U(\mathbf{r})}{kT}\right]} . \tag{2.5}$$

Here N_Σ is the number of spheres on a given plane, each plane being identical and having dimensions $L\times L$, and the polarization of the array is $\mathbf{P}_{NL}(\mathbf{r},t)=\alpha n(\mathbf{r})\mathbf{E}(\mathbf{r},t)$. The spacing between each plane being L/N_z.

B. Third-order susceptibility for translational optomechanical arrays

For a single beam of frequency ω, phase $\phi(\mathbf{r})$, propagation vector $\mathbf{K}$, polarization vector $\mathbf{e}$, and amplitude $E_0 a(\mathbf{r})$, the electric-field component $\mathbf{E}(\mathbf{r},t)=\mathbf{e}E_0 a(\mathbf{r})\cos[\mathbf{K}\cdot\mathbf{r}-\omega t+\phi(\mathbf{r})]$. We have

$$\frac{U(\mathbf{r})}{kT}=-\frac{1}{4}\frac{\epsilon_B-1}{\epsilon_B+2}E_0^2\frac{r_0^3a^2(\mathbf{r})}{kT}\equiv -ga^2(\mathbf{r}) , \tag{2.6}$$

where the dimensionless parameter $g\equiv\xi r_0^3E_0^2/4kT$ governs the strength of the particle-field coupling and $\xi\equiv(\epsilon_B-1)/(\epsilon_B+2)$. The spatial distribution of particles is $n(\mathbf{r})$ with $\mathbf{r}$ in the plane of the spheres, since the beam is confined to lie in the plane of the particles (xy plane)

$$n(\mathbf{r})=n_0\frac{\exp[ga^2(\mathbf{r})]}{\dfrac{1}{V}\int d^3r\exp[ga^2(\mathbf{r})]} \tag{2.7}$$

and the spheres will congregate where the beam is most (least) intense if $\alpha>0$ ($\alpha<0$, i.e., $-2\le\epsilon_B\le 1$). If the beams are uniform and extend over the entire array, $n(\mathbf{r})=n_0$, i.e., the particle density is spatially homogeneous in the plane of the particles.

The polarization of the array is

$$\mathbf{P}(\mathbf{r},t)=\frac{3f}{4\pi}\frac{\epsilon_B-1}{\epsilon_B+2}\frac{\exp[ga^2(\mathbf{r})]}{\dfrac{1}{V}\int d^3r\exp[ga^2(\mathbf{r})]}\mathbf{E}(\mathbf{r},t) , \tag{2.8}$$

where $f\equiv 4\pi r_0^3n_0/3$ is the volume fraction of spheres. Note that if the beam is spatially uniform, then there is no electrostrictive force and $\mathbf{P}(\mathbf{r},t)$ is linear:

$$\mathbf{P}(\mathbf{r},t)=\frac{3f}{4\pi}\frac{\epsilon_B-1}{\epsilon_B+2}\mathbf{E}(\mathbf{r},t) . \tag{2.9}$$

For a spatially varying beam in the weak-field limit, we can expand Eq. (2.8) in powers of g and extract the various nonlinear-optical susceptibilities. An examination of Eq. (2.8) reveals that these expansions involve spatial integrals of different powers of the shape factor $a^2(\mathbf{r})$. For example, if $g \ll 1$, the third-order polarization is

$$\mathbf{P}_{\rm NL}^{(3)}(\mathbf{r},t)=\frac{3f}{16\pi}\left[\frac{\epsilon_B-1}{\epsilon_B+2}\right]^2\frac{r_0^3}{kT}\langle\delta a^2(\mathbf{r})\rangle a(\mathbf{r})E_0^3 , \quad (2.10)$$

where $\langle\delta a^2(\mathbf{r})\rangle$ is the mean-square spatial deviation of the beam, i.e., $\langle\delta a^2(\mathbf{r})\rangle\equiv a^2(\mathbf{r})-\langle a^2(\mathbf{r})\rangle$. If the third-order optical susceptibility is to be local, it can be defined in the following manner: $\mathbf{P}_{\rm NL}^{(3)}(\mathbf{r},t)=\chi^{(3)}\langle\delta\mathbf{E}^2(\mathbf{r},t)\rangle\mathbf{E}(\mathbf{r},t)$, where

$$\chi^{(3)}=\frac{3f}{16\pi}\left[\frac{\epsilon_B-1}{\epsilon_B+2}\right]^2\frac{r_0^3}{kT} . \quad (2.11)$$

For an array composed of 10μm (100 μm) -sized metallic or metal-coated spheres and a volume fraction of 10^{-4}, $\chi^{(3)}=0.149$ esu (149.2 esu) at $T=300°$ K.

C. Response to a static electromagnetic grating

We examine the case of two degenerate, cw monochromatic, plane-wave beams of frequency ω, polarized in the xy plane and coherently interfering inside a translational optomechanical array:

$$\mathbf{E}(\mathbf{r},t)=E_0\sum_{m=1}^{2}\mathbf{e}_m b_m\exp[i(\mathbf{K}_m\cdot\mathbf{r}-\omega t+\varphi_m)]+\text{c.c.} , \quad (2.12)$$

where $\mathbf{e}_m$, $E_0 b_m$, φ_m, and $\mathbf{K}_m$ are, respectively, the unit polarization vector, amplitude, phase, and propagation vector of the mth beam. The interaction of these two beams with a given sphere located at the point $\mathbf{r}$ in the array is

$$\frac{U(\mathbf{R})}{kT}=-\frac{g}{4}\{b_1^2+b_2^2+b_1b_2\mathbf{e}_1\cdot\mathbf{e}_2\exp[i(\mathbf{Q}\cdot\mathbf{r}+\phi)]+\text{c.c.}\} , \quad (2.13)$$

where $\phi\equiv\phi_1-\phi_2$ and $\mathbf{Q}\equiv\mathbf{K}_1-\mathbf{K}_2$. For plane-wave beams that extend well beyond the dimensions of the array, the self-interaction terms give rise to only a phase shift and can be ignored. This leaves the grating term which orders the spheres in accordance to

$$n(\mathbf{r})=n_0\frac{\exp[gb_1b_2\cos(\mathbf{Q}\cdot\mathbf{r}+\phi)]}{I_0(gb_1b_2)} , \quad (2.14)$$

where $I_k(z)$ is modified Bessel function of order k, argument z and $\mathbf{r}$ is located on one of the planes. The sphere density $n(\mathbf{r})$ can be decomposed into various grating orders, and denoting the component of order k by $n_k(\mathbf{r})$, we have

$$n(\mathbf{r})=\sum_{k=0}^{\infty}n_k(\mathbf{r})\equiv\sum_{k=0}^{\infty}m_k\cos[k(\mathbf{Q}\cdot r+\phi)](2-\delta_{k0}) . \quad (2.15)$$

Here $m_k\equiv 2n_0 I_k(gb_1b_2)/I_0(gb_1b_2)$ is the amplitude of the kth-order index grating. For small g, $m_k\propto g^k$. For $g\to\pm\infty$, $m_k\to 2n_0$ and the particle density approaches

$$n(\mathbf{r})=N\sum_j\sum_l\sum_p\delta(x-x_j)\delta(y-y_l)\delta(z-z_p) , \quad (2.16)$$

where N is the total number of spheres and (x_j,y_l) are points where $U(\mathbf{r})$ is a minimum and z_p is a plane coordinate. This is the expected density for a purely mechanical system in which the spheres reside at the points where the electrostrictive force is zero. For 10-μm-sized metallic or metal-coated spheres, $g=104.7\,(I_1I_2)^{1/2}$, where I_1 and I_2 are the beam intensities in W/cm^2. For 100-μm spheres $g=1.047\times10^5\,(I_1I_2)^{1/2}$. Unless the power densities are very low, g will be quite large and numerous higher-order index gratings will be generated.

Next, we evaluate the nonlinear susceptibilities of an array that has been irradiated by two degenerate plane-wave electromagnetic beams. Specifically, we determine the polarization sensed by a probe (or read) beam, $\mathbf{E}_p(\mathbf{r},t)\equiv\mathbf{e}_p\mathcal{E}_p\cos[k(\mathbf{K}\cdot\mathbf{r}-\omega t)]$ that is diffracted by the kth-order optical index grating created within the array by the write beams. More precisely, we evaluate $\mathbf{P}_{\rm NL}^{(k)}(\mathbf{r},t)\equiv\alpha n_k(\mathbf{r})\mathbf{E}_k(\mathbf{r},t)\equiv\chi_{\rm NL}^{(k)}\mathbf{E}(\mathbf{r},t)$ which using Eq. (2.15) is given by

$$\mathbf{P}_{\rm NL}^{(k)}(\mathbf{r},t)=\frac{3f}{4\pi}\frac{\epsilon_B-1}{\epsilon_B+2}\frac{I_k(gb_1b_2)}{I_0(gb_1b_2)}\mathbf{e}_p\mathbf{E}_p . \quad (2.17)$$

If $\mathbf{E}_p(\mathbf{r},t)$ is the kth harmonic of the two write beams, I_1 and I_2, the saturated nonlinear-optical susceptibility associated with the kth-order index grating $\chi_{\rm NL}^{(k)}$ is, with $b_1=b_2=1$,

$$\chi_{\rm NL}^{(k)}=\frac{3f}{4\pi}\frac{\epsilon_B-1}{\epsilon_B+2}\frac{I_k(g)}{I_0(g)} . \quad (2.18)$$

In the limit $g\to0$, the nonlinear-optical susceptibility associated with the kth-order index grating, approaches g^k and $\chi_{\rm NL}^{(1)}\to\chi^{(3)}$. Note that for $g\gg1$, $\chi_{\rm NL}^{(k)}\to n_0\alpha=3f/4\pi=n_0r_0^3$ for a metal-coated particle. Thus, for 10-μm-sized metal spheres, such as aluminum or copper, $\alpha\to10^{-9}$ cm^3, whereas for 100-μm-sized spheres, $\alpha\to10^{-6}$ cm^3. If the volume fraction is 10^{-2}, then $\chi_{\rm NL}^{(k)}\to2.4\times10^{-3}$ esu. Note that for beam intensities of 1 W/cm^2, g ranges from 1.047×10^2–1.047×10^5 as r_0 varies from 10 to 100 μm. Thus the medium will clearly generate many higher-order index gratings. Furthermore, such large values of g at low beam powers imply that the medium is relatively easy to saturate. In particular, for 100-μm-sized metallic spheres and write beam intensities on the order of mW/cm^2, $g=104.7$, and the first 50 or so index grating orders achieve their saturated values.

Figure 1 depicts the nonlinear-optical susceptibilities associated with the first five index gratings versus write beam intensities, i.e., $I_{\rm beam}=(I_{\rm sig}I_{\rm pump})^{1/2}$ with $I_{\rm sig}$ ($I_{\rm pump}$) the signal (pump or reference beam) intensity. The calculation for Fig. 1 assumed that the medium is composed of 10-μm-sized metallic spheres, with $f=10^{-4}$. Here the numbers specify the grating order and the dimensionless saturation parameter $g=104.71_{\rm beam}$, where

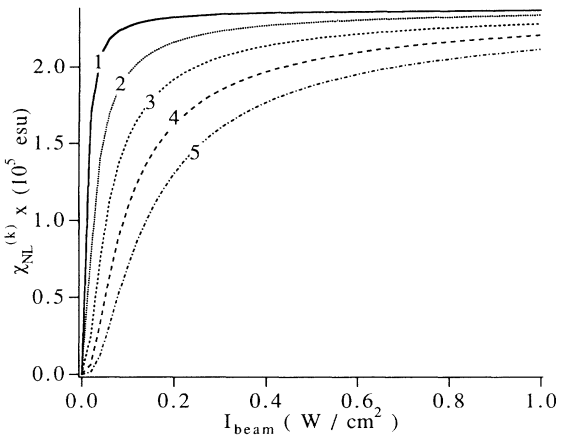

FIG. 1. $\chi_{NL}^{(k)}$ for the first five index grating vs I_{beam} intensity for 10-μm metallic spheres with $f=10^{-4}$.

I_{beam} is measured in W/cm^2. Thus, $g \approx 10$ for $I_{beam}=0.1$ W/cm^2 and an examination of this figure reveals that $\chi_{NL}^{(1)}=\chi^{(3)}$ saturates at these write beam intensities. Also, $\chi_{NL}^{(2)}$ saturates at beam intensities on the order of 0.2 W/cm^2 and $\chi_{NL}^{(3)}$ saturates at beam intensities on the order of 0.3 W/cm^2. Hence, the nonlinear-optical susceptibilities associated with the higher-order index gratings are smaller than the lower-order ones and require higher beam intensities to saturate. However, it is clear that all of the lower-order gratings saturate at intensities on the order of 1 W/cm^2 and approach a limiting value set by the volume fraction of spheres; specifically, $3f/4\pi$. If the medium is composed of 100-μm-sized metallic or metal-coated spheres, the dimensionless saturation parameter $g=104.71_{beam}$, where I_{beam} is now measured in mW/cm^2. Thus, $g \approx 10$ for $I_{beam}=0.1$ mW/cm^2 and the first-order index grating saturates at intensity levels on the order of 100 μW/cm^2. A similar statement is true for the other index gratings, and the nonlinear susceptibilities of the lower-order index gratings will all saturate at microwave beam intensities on the order of several hundred μW/cm^2.

Finally, the scattering attenuation length (L_S) is also an important parameter for optical phase conjugation, since the propagation length L must be much smaller than L_S, if scattering losses are to be avoided. The scattering attenuation length in the Rayleigh regime is given by

$$L_s^{-1}=\frac{256\pi^5 n_0 \alpha^2}{\lambda^4} \overset{\text{metal}}{\rightarrow} \frac{326\pi^4 f r_0^3}{\lambda^4} . \tag{2.19}$$

For 10-μm (100-μm) -sized metal spheres irradiated by 1-mm (3-mm) radiation, $L_S > 3.2\times10^4$ cm ($L_S > 2\times10^3$ cm) for $f=10^{-3}$ and scattering is negligible. Note that in the unsaturated regime, where $g \ll 1$, the parameter $\chi^{(3)}L_S$ depends only on wavelength and temperature:

$$\chi^{(3)}L_s=\frac{3}{256\pi^4}\left[\frac{\lambda^4 I_{beam}}{ckT}\right] . \tag{2.20}$$

Now I_{beam} scales as λ^{-2}, thus $\chi^{(3)}L_S$ scales as λ^2, and it follows that translational Kerr media are most suitable for long-wavelength applications.

III. TRANSIENT DYNAMICS OF A ROLLING SPHERE

In this section we investigate the transient dynamics of a sphere that is free to roll on a flat, transparent plane. Before proceeding further, we first determine what restrictions are placed on plane alignment to ensure that gravity is negligible. Gravity is insignificant if the electrostrictive force is much greater than the component of the gravitational force that retards the rearrangement of the sphere. Thus, we require $4\pi\alpha(\partial/\partial z)I_{beam}/c > mg\sin\theta$, where α is the polarizability of the sphere, θ is the angle of the support structure with respect to the vertical, I_{beam} is the beam intensity, g is the gravitational acceleration, and m is the particle's mass. If the length scale over which the I varies is ℓ, then $\theta \ll \sin^{-1}[4\pi\alpha I_{beam}/c\ell mg]$. For metal-coated particles, this reduces to $\theta \ll 4\pi I_{beam}/c\ell\rho g$, where ρ is the mass density of the sphere. For $\ell=1$ mm, $I_{beam}=10$ W/cm^2 and $\rho=1$ g/cm^3, $\theta \ll 1.2\times10^{-2}$°; i.e., the support structure must be normal with the vertical direction to within a few tenths of a milliradian. Note that vibration isolators will be required to ensure that the gratings are not destroyed by vibrations.

A. Equations of motion

We now turn to the transient dynamics of a rolling sphere and first explicitly construct its Langevin equation of motion. We assume that the support structure is sufficiently aligned that gravitational forces can be neglected. The sphere is subject to an electrostrictive force, $\mathbf{F}=-\nabla U$, reaction forces $\mathbf{R}$ arising from surfaces in contact with the sphere and friction forces $\mathbf{F}_f$ from both air and the mechanical support structure. Figure 2 depicts the situation of interest.

Let $\mathbf{V}$ be the translational velocity of the sphere and Ω its angular velocity. Then the velocity $\mathbf{v}$ at the point of contact of the sphere with the plane is

$$\mathbf{v}=\mathbf{V}-r_0\Omega\times\hat{\mathbf{z}} . \tag{3.1}$$

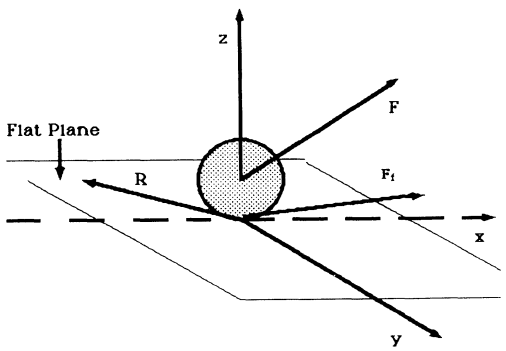

FIG. 2. A sphere rolling on a perfectly rough, flat plane and subject to electrostrictive and frictional forces and torques.

We assume that the plane is perfectly rough, i.e., the sphere does not slide, so that $\mathbf{v}=0$. Thus we have the following constraint:

$$\mathbf{V}=r_0\Omega\times\hat{\mathbf{z}} \ . \tag{3.2}$$

The equations of motion for an individual sphere rolling on a perfectly rough plane are specified by d'Alembert's principle:

$$m\frac{d\mathbf{V}}{dt}=\mathbf{F}'+\mathbf{R} \ , \tag{3.3a}$$

$$I\frac{d\Omega}{dt}=\mathbf{K}_f-r_0\hat{\mathbf{z}}\times\mathbf{R} \ , \tag{3.3b}$$

where $\mathbf{F}'=\mathbf{F}+\mathbf{F}_f$, $\mathbf{F}_f(\mathbf{K}_f)$ is the frictional force (torque) exerted on the sphere by air, and $I=2mr_0^2/5$ is the sphere's moment of inertia. To solve Eqs. (3.3) for the motion of the sphere, we require an expression for the reaction force $\mathbf{R}$. Differentiating the constraint equation and substituting into Eq. (3.3a) and using Eq. (3.3b) to eliminate Ω, we get

$$\left[\frac{I}{r_0m}\right](\mathbf{F}'+\mathbf{R})=\mathbf{K}\times\hat{\mathbf{z}}-r_0\mathbf{R}+r_0\hat{\mathbf{z}}(\hat{\mathbf{z}}\cdot\mathbf{R}) \ . \tag{3.4}$$

Next we require the frictional forces and torques that the sphere encounters as it rolls on the plane. These are drag and rolling friction of the sphere with the plane. For a sphere moving slowly through a viscous fluid (e.g., air),

$$\mathbf{F}_f=-6\pi\eta r_0\mathbf{V} \ , \tag{3.5}$$

where η is the dynamic viscosity of air ($1.8\times10^{-4}p$ at STP). Also, a sphere rotating in an incompressible fluid or gas with a uniform angular velocity Ω experiences a frictional torque

$$\mathbf{K}_f=-8\pi\eta r_0^3\Omega \ . \tag{3.6}$$

The rolling friction from the plane is

$$\mathbf{K}_r=-\mu_r r_0 mg\hat{\mathbf{z}}\times\hat{\mathbf{r}} \ , \tag{3.7}$$

where μ_r is the coefficient of rolling friction. The sphere is also subject to a fluctuating Langevin force $\Gamma(t)$ that is associated with the dissipation due to friction. The Langevin equation of motion for a given sphere is

$$\frac{d\mathbf{V}}{dt}=-\frac{5}{7m}\left[\nabla U(\mathbf{r},t)+\mu_R mg\frac{\mathbf{V}}{V}\right]-\frac{52\pi}{7m}\eta r_0\mathbf{V}+\Gamma(t) \ . \tag{3.8}$$

Typically, μ_R is negligible, i.e., $\mu_R\approx0.1\%$ and can be ignored.

B. Decay of particle velocity

We first examine the response of the system in the absence of external fields. Setting $U=0$, ignoring thermal fluctuations and rolling friction, we find that if the sphere is initially moving at a velocity $\mathbf{V}$, its subsequent motion is

$$\mathbf{V}(t)=\mathbf{V}_0\exp(-t/\tau) \ , \tag{3.9}$$

where $\tau=(7\rho r_0^2/39\pi\eta)$. For 100-$\mu$m-sized spheres, with $\rho=1$ g/cm^3 and the array sited in air at STP, $\tau=99.7$ ms. Note that the decay time scales directly with particle surface area and mass density and inversely with medium viscosity; i.e., a typical diffusive response.

C. Particle dynamics in a static electromagnetic grating

Next we examine the motion of an individual sphere subject to electrostrictive forces generated by a static electromagnetic index grating created by two coherently interfering degenerate, cw plane-wave beams. The electrostrictive potential is given by Eq. (2.13) and the associated force is $\mathbf{F}=-\mathbf{Q}gkT\sin[\mathbf{Q}\cdot\mathbf{r}]$. The equation of motion for an individual sphere is

$$\frac{d\mathbf{V}}{dt}+\frac{52\pi}{7m}\eta r_0\mathbf{V}+\frac{5\alpha\mathbf{E}_1\cdot\mathbf{E}_2}{14m}\mathbf{Q}\sin[\mathbf{Q}\cdot\mathbf{r}]=\Gamma(t) \ . \tag{3.10}$$

The acceleration that a copper sphere experiences is independent of its size, and for 10-W/cm^2 counterpropagating beams is 0.024 cm/s^2, i.e., $\approx239\mu$ gravities. The total force on a 100-μm-sized copper ($\rho=8.96$ g/cm^3) sphere is on the order of 0.13 μdyn. The equation of motion for an individual particle rolling on a perfectly flat plane with $\mu_R=0$, under the action of the forces discussed above can be written in the form

$$\ddot{\xi}+2\beta\dot{\xi}+\omega_0^2\sin\xi=N(t) \ . \tag{3.11}$$

Here, $\mathbf{Q}$ defines the x direction, $\beta\equiv39\eta/14\rho r_0^2$, $\xi(t)\equiv Qx(t)$, $N(t)\equiv Q\Gamma(t)$. The grating spacing $\Lambda=2\pi/Q$, $\omega_0\equiv(2\pi/\Lambda)(15I_{\rm beam}/7\rho c)^{1/2}$ and $I_{\rm beam}\equiv(I_pI_1)^{1/2}$. In particular, $\langle N(t)\rangle=0$ and $\langle N(t)N(t')\rangle=2kTQ^2\beta\delta(t-t')/m$. For situations of interest to us, the particle's motion is dominated by the electrostrictive force and dissipation arising from air friction.

Examination of the equation of motion reveals three regimes of interest: (i) an oscillatory underdamped regime, (ii) an overdamped regime, and (iii) a diffusive regime. In the oscillatory regime, where $\omega_0\gg\beta$, the time it takes for the medium to achieve steady state (τ_R) is β^{-1}, while ω_0 is the resonant frequency. In the overdamped regime, $\omega_0\ll\beta$, the medium response time $\tau_R=2\beta/\omega_0^2$ and for metallic spheres $\tau_R^{-1}\equiv Q^2(15r_0^2I_{\rm beam}/39\eta c)$. Finally, the particle is in the diffusive regime if the Langevin force exceeds the electrostrictive force, i.e., $U/kT\ll1$. This occurs if $\pi r_0^3I_{\rm beam}/30\ll1$, where r_0 is in μm and $I_{\rm beam}$ in W/cm^2. For this situation analysis of Eq. (3.11) shows that $1/\tau_R\approx21kT(2\pi/\Lambda)^2/156\pi\eta r_0$.

1. *Overdamped regime without noise*

In this regime the inertia term is negligible and Eq. (3.11) can be solved analytically in the absence of the Langevin noise term

$$\sin[\xi(t)]=\frac{\sin[\xi(0)]e^{-t/\tau_R}}{\{1-\sin^2[\xi(0)](1-e^{-t/\tau_R})\}^{1/2}} \ . \tag{3.12}$$

An examination of Eq. (3.12) shows that the particle rolls from its initial position $\xi(0)$ into its equilibrium position on a time scale set by τ_R. Note that the inverse response time in Eq. (3.12) can be cast in the following form: $1/\tau_R \approx D'(2\pi/\Lambda)^2(U/kT)$, with $D'=15kT/156\pi\eta r_0$ the translational diffusion coefficient for a sphere moving in a medium with a viscosity η. This should be contrasted with a suspension in the strong-field regime, where the medium response time [5] $\tau_R^{-1}=DK^2(U/kT)$, with $D=6\pi kT/r_0\eta$ being the translational diffusion coefficient for a sphere in a viscous fluid. We will return to this point in the next section, where we study the transient dynamics of an array of spheres.

The particle response time $\tau_D=3.56\times10^{-2}[r_0/\lambda\sin(\theta/2)]^2 I_{\text{beam}}$, where I_{beam} is in W/cm^2 and the sphere is sited in air at STP. If the radiation wavelength is 3 cm, the particles are 100-μm copper spheres and the angle between the beams is 90°, then $\tau_D=6.41$ s for beam intensities of 100 W/cm^2. For 18-GHz radiation and the same beam powers and propagation directions, the medium response time will be on the order of 174 s. The optical response time for the formation of a translational grating in a carbon fiber microparticle suspension at these wavelengths and particle sizes is on the order of several h to a few d [6]. Finally, although the medium response time scales inversely with the dynamic viscosity of the air, decreasing the air pressure will not necessarily reduce the medium response time. In particular, the dynamical viscosity [13] of a gas is given by $\eta=\frac{1}{3}nv_{\text{th}}m\ell$. Here n is the density of gas molecules, v_{th} is their thermal velocity, and ℓ is the molecular mean-free path. Now, since $\ell\approx1/n\sigma_0$, where σ_0 is the cross section for elastic collisions, the gas viscosity is independent of gas pressure. This remains valid so long as $\ell<L$, the dimensions of the container. Since $\sigma_0\approx10^{-15}$ cm^2, this statement is true so long as $n>10^{13}$/cm^3, i.e., for gas pressures greater than 1 mtorr.

2. *Underdamped regime without noise*

Next we examine the underdamped region, again in the absence of thermal fluctuations. Figure 3 depicts the transient behavior of $\sin[\xi(t)]$ for a 100-μm metal-coated sphere with $\rho=0.2$ g/cm^3. For this case $\omega_0^2/2\beta=14.1$-s for a beam intensity of 0.5 W/cm^2. The particle is initially placed at $\xi(0)=1.0$ and the radiation beams are such that the grating spacing $\Lambda=1$ mm. The calculation examines the transient motion of a rolling sphere until it achieves steady state. An examination of the figure reveals that the particle overshoots the equilibrium point ($\xi_{\text{eq}}=0$) and oscillates about it a number of times before coming to rest. The time scale for this motion is on the order of 10 s, in good agreement with the value of $2\beta=1.01$ s^{-1}. Furthermore, $\omega_0=3.75$ s^{-1}, implying an oscillation period of 0.26 s.

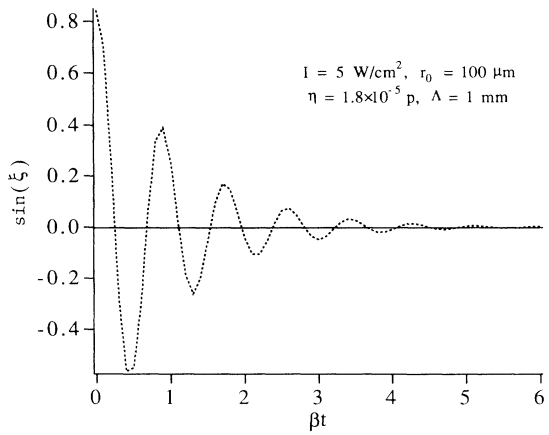

FIG. 3. Motion of a sphere in the underdamped case.

3. *Manifestation of noise in the overdamped regime*

Next we examine how noise manifests itself in the sphere's motion. The Langevin equation of motion for a given particle is

$$\ddot{\xi}+2\beta\dot{\xi}+\omega_0^2\sin\xi=N(t)\ . \tag{3.13}$$

The deviations that the particle undergoes from thermal fluctuations arising from collisions with air molecules is small. Thus we decompose the particle position into a deterministic piece, $\xi_D(t)$ plus a random fluctuating term $\delta\xi(t)$, i.e., $\xi(t)=\xi_D(t)+\delta\xi(t)$. These satisfy

$$\ddot{\xi}_D+2\beta\dot{\xi}_D+\omega_0^2\sin\xi_D=0\ , \tag{3.14a}$$

$$\delta\ddot{\xi}+2\beta\delta\dot{\xi}+(\omega_0^2\cos\xi_D)\delta\xi=N(t)\ . \tag{3.14b}$$

In steady state, $\xi_D(t)=2n\pi$, and solving Eq. (3.14b) yields the stochastic motion of the particle under equilibrium conditions

$$\delta\xi(t)=-\int_{-\infty}^{\infty}d\omega\, e^{i\omega t}\frac{N(\omega)}{\omega^2-2i\beta\omega-(\omega_0^2\cos\xi_D)}\ . \tag{3.15}$$

The magnitude of the noise varies inversely with the particle mass and increases with temperature. In particular, in the overdamped regime the rms position fluctuation of a particle, $\langle(\delta x)^2\rangle^{1/2}=(kT/m\omega_0^2)^{1/2}$ and scales as the

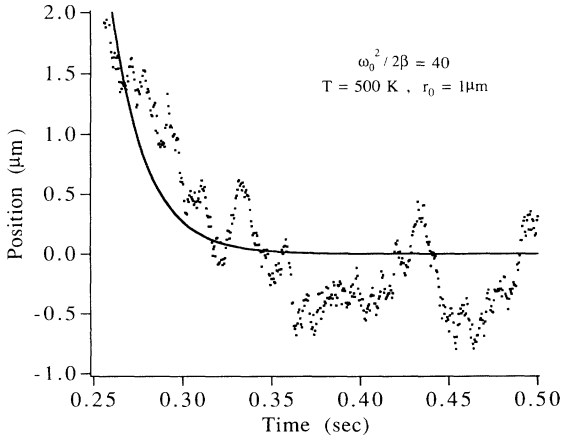

FIG 4. Transient motion of a 1-μm-sized sphere undergoing Brownian motion in a static index grating.

thermal velocity of a sphere $[(kT/m)^{1/2}]$ divided by the oscillation frequency. Typical thermal velocities at room temperatures for a 100-μm-sized metallic sphere are 10^{-4} cm/s and for a beam intensity of 1 W/cm^2, $\omega_0=0.7$ s. Thus $\langle(\delta x)^2\rangle^{1/2}=1$ μm.

Figure 4 depicts the case of a 1-μm metal-coated particle maintained in 760-Torr pressure and irradiated with equal beam intensities of 1 MW/cm^2. The particle is taken have a mass density $\rho=1$ g/cm^3, a grating spacing $\Lambda=1$ mm, $T=500$ K, $\omega_0=1680$ s^{-1}, $\beta=2.8\times10^4$, and $\omega_0^2/2\beta=40$. In Fig. 4, the solid line tracks the position of the sphere in the absence of noise and the dots represent the sphere's position with noise present. An examination of the particle's motion indeed reveals that Brownian fluctuations cause the particle to move randomly over distances on the order of half of a μm, i.e., $\langle(\delta x)^2\rangle^{1/2}\approx1$ μm.

IV. TRANSIENT DYNAMICS OF THE ARRAY

Next we examine the transient dynamics of an entire array of rolling spheres. In Sec. IV A we study the time evolution of the sphere density by adding up the contribution to $n(\mathbf{r},t)$ of the motion of each individual sphere. We refer to this as the Monte Carlo approach. In Sec. IV B, we examine the time evolution of the translational optical index grating created by the spheres as they are driven to their equilibrium positions by electrostrictive forces. We investigate the effect of the initial particle distribution on transient index grating dynamics and the impact of thermal fluctuations. Finally, in Sec. IV C we inspect grating dynamics for the overdamped case from the perspective of the Planck-Nernst equation. This is the standard approach used for describing microparticle suspension dynamics. We find by direct comparison that the Monte Carlo and Planck-Nernst approaches give essentially the same description of optomechanical grating dynamics in this regime.

A. Time evolution of the particle density

At the time $t=0$, the radiation beams are switched on and the ensemble is allowed to progress towards steady state. The dynamics of each particle, which is governed by Eq. (3.11), is determined and the transient behavior of $n(\mathbf{r},t)$ is obtained by a Monte Carlo approach in which we sum over the entire set of spheres. To simplify matters, we restrict the calculation to a single plane and evaluate the evolution of the sphere density along the Q direction. Note that in the absence of dissipation the spheres never achieve steady state, and if they were initially randomly positioned, a coherent density grating will never form.

1. Evolution of the density in the overdamped case

We examined the transient dynamics of a system of 1000 identical metallic spherical particles that are irradiated by two cw, plane-wave degenerate beams. The sphere size, air density, and beam intensity are such that the system is in the overdamped regime for the case $g=4\pi r_0^3 I_{\text{beam}}/ckT=122.5\pi$. As a specific numerical example, consider 1000, 15-μm-sized metal-coated spheres with $\rho=2$ g/cm^3, irradiated by two degenerate write beams with $I_{\text{beam}}=1$ W/cm^2 and a grating period of 1 mm. For these system parameters, $\tau_D=632$ s. If the particle size is increased to 150 μm, then write beam intensities of 0.1 W/cm^2 will give the same value of g and grating formation will occur on a time scale of 6.3 s. Our results for the sphere density are presented in Figs. 5, which depicts $n(\xi,t)$ versus t/τ_D. Here $\xi=Qx$, $\tau_D^{-1}\equiv15(Kr_0)^2I_{\text{beam}}/39\eta c$ and the density was calculated by dividing the region of space (equal to two complete grating periods) into 50 subunits and counting the number of particles in each subunit. Figure 5(a) depicts the transient evolution of $n(\xi,t)$ over the spatial region $0\le\xi\le4\pi$ at the times $t/\tau_D=0$, 0.5, 1.0, and 1.5. Initially the spheres are randomly distributed and this is reflected by the essentially flat nature of the density at the time $t=0$. The small irregularities arise from the fact that the sample involves a finite number of particles and this gives rise to a local fluctuations due to the discrete nature of the system. After the beams are turned on, the particles are attracted to the regions where the radiation intensity is greatest, i.e., $\xi=2n\pi$, with $n=0,\pm1,\pm2$, etc.,

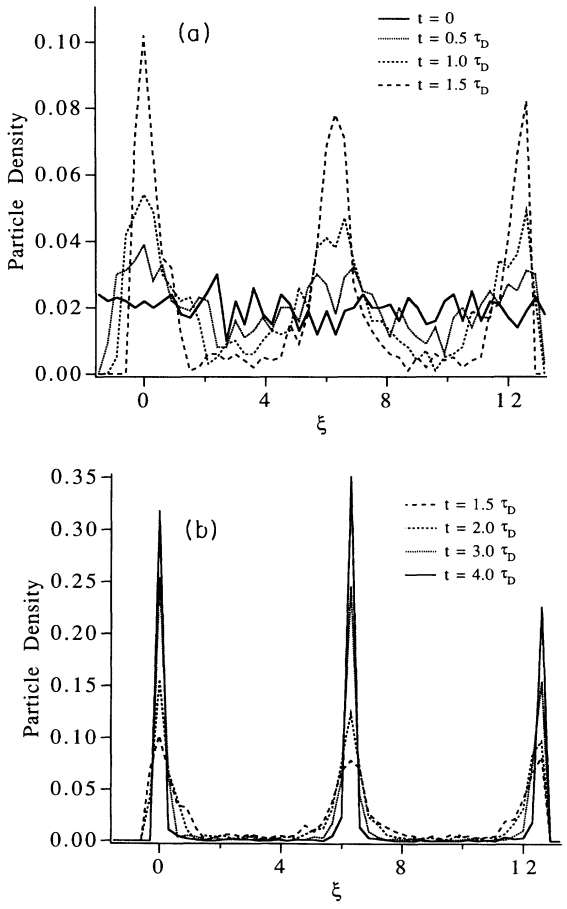

FIG. 5. (a) Transient motion of $n(\xi,t)$ vs t/τ_D in a static index grating after the fields are turned on. (b) Transient motion of $n(\xi,t)$ vs t/τ_D in a static index grating approaching the steady-state distribution.

on a time scale set by τ_D. Thus, by $t/\tau_D=1.0$, there is a definite clumping of the spheres in the vicinity of where the electrostrictive force is zero. By $t/\tau_D=1.5$, this clumping is very noticeable and the particle spatial distribution is rapidly depleted from the regions where the electrostrictive force is strongly repulsive, i.e., $\xi=(2n+1)\pi/2$. Figure 5(b) continues this description of $n(\xi,t)$ for the times $1/\tau_D=2.0$, 3.0, and 4.0. An examination of the particle density during these times reveals that the density is rapidly achieving equilibrium with the

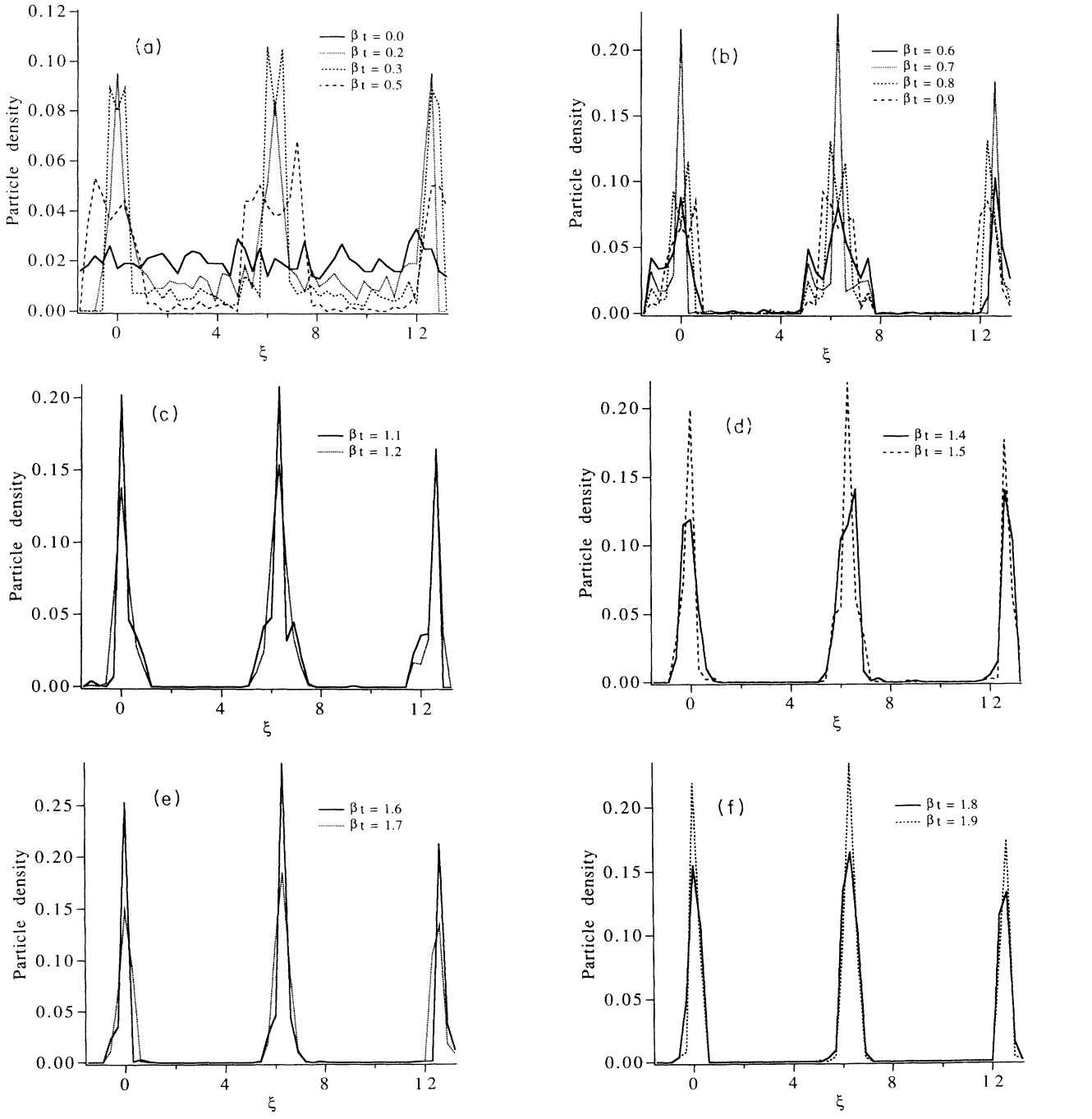

FIG. 6. (a) Early transient behavior of the sphere density over two grating spacings for the system in an underdamped state. (b) Intermediate transient behavior if the sphere density over two grating spacings for the system in an underdamped state. (c) Intermediate transient behavior if the sphere density over two grating spacings for the system in an underdamped state. (d) Intermediate transient behavior if the sphere density over two grating spacings for the system in an underdamped state. (e) Intermediate transient behavior if the sphere density over two grating spacings for the system in an underdamped state. (f) Intermediate transient behavior if the sphere density over two grating spacings for the system in a underdamped state. (g) Final achievement of steady state by the sphere density over two grating spacings for the system in an underdamped state.

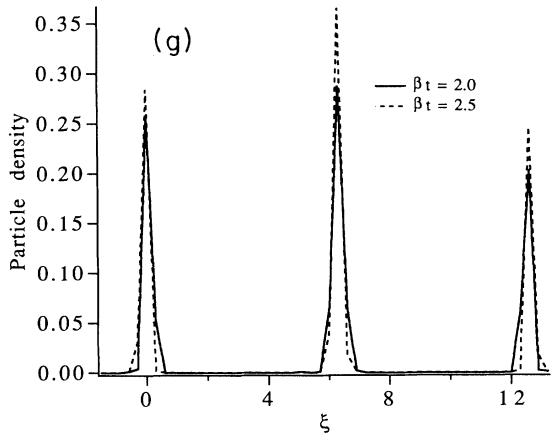

FIG. 6. (*Continued*).

particles strongly bunched in the regions $\xi=2n\pi$. Note, too, that the spatial distribution is not even about these points. This feature of particle dynamics arises from the fact that there were more particles closer to $\xi=0$ and 2π than to $\xi=4\pi$ at $t=0$.

2. *Evolution of the density in the underdamped case*

Next we examine the transient dynamics of the sphere density in the underdamped case, where the individual particle motion exhibits oscillations about the equilibrium position. On physical grounds we anticipate that the particle density will reflect these oscillations.

We investigate the specific case in which 1000, 100 μm-sized metal-coated spheres with $\rho=0.1$ g/cm^3 are irradiated by two degenerate radiation beams with $I_{\text{beam}}=0.5$ W/cm^2. The grating spacing is 1 mm and the spheres are initially placed randomly on the plane, with zero velocity. The array decay time $\beta=0.5$ s^{-1}. The medium should form the translational index gratings on a time scale set by 2 s and $\omega_0=3.75$ s^{-1}, so that the oscillations period is 0.26 s. Figures 6(a)–6(g) depict the transient evolution of the particle density for the time interval of $0\leq\beta t\leq 2.5$, after which we find that there are no detectable changes in $n(\xi,t)$ and the system has achieved steady state. The spatial range of the calculation covers two complete grating spacings.

Figure 6(a) depicts the earlier dynamics of the system with the sphere density initially random. An examination of this figure reveals that the spheres immediately start to congregate about their equilibrium positions $\xi=0$, 2π, and 4π. By $\beta t=0.3$, the spheres are well localized about these points. Note that even during early times the distribution exhibits some oscillations. For example, the density appears to become more localized for $0\leq\beta t\leq 0.3$; however, the peaks around $\xi=0$, 2π, and 4π decrease and the distribution spreads in space afterwards. For example, by $\beta t=0.5$, the density falls to about one-half of its value at $\beta t=0.3$ and is spread over a much broader region.

Figure 6(b) depicts the time interval $0.6\leq\beta t\leq 0.9$, where the same behavior is repeated, only the distribution is somewhat closer to steady state and the particle density is more localized about the equilibrium points. Note that at the time $\beta t=0.7$, the sphere density achieves a value around the equilibrium points that is more than 50% of its final value.

Figure 6(c) depicts the evolution of the sphere density for the times $\beta t=1.1$ and 1.2. By this time there are very few spheres left in the regions between the equilibrium points. Note that the density is still oscillating, with $n(\xi,t)$ achieving values that are on the order of one-half of the steady state value at the equilibrium points. Figures 6(d)–6(f) exhibit the same general behavior with the density oscillating in magnitude about the equilibrium points and the region between these points being essentially devoid of spheres. Finally, Fig. 6(g) depicts the assumption of steady state in a time interval of $t=2.0/\beta$ and $2.5/\beta$.

B. Index grating formation: Monte Carlo approach

Now, as discussed in the previous section, under the action of a periodic potential, $\cos(\mathbf{Q}\cdot\mathbf{r})$, the particle density will evolve into various grating components, i.e., $\cos(n\mathbf{Q}\cdot\mathbf{r})$, with n an integer. Further, the effective nonlinear polarization responsible for optical phase conjugation is determined by the ensemble average of the first-order grating function over the particle distribution. Thus it is of interest to study the time evolution of the grating function

$$y(t)\equiv\frac{\sum_{k=1}^{N} n(\xi_k,t)\cos\xi_k}{N}\ , \tag{4.1}$$

where N is the total number of particles. In steady state, the grating is saturated if $g\gg 1$ and $y\rightarrow 1$, since all of the particles are located at points where the grating function, $\cos\xi(t)$, is unity.

1. *Evolution of the grating in the overdamped case*

Figure 7 depicts the time evolution of the grating function $y(t)$ for the specific overdamped case used in Fig. 5. For the situation examined here, the particles were ini-

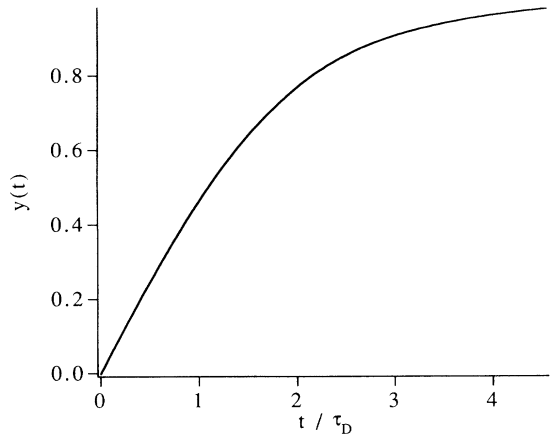

FIG. 7. Time evolution of the particle grating function vs t/τ_d for the overdamped case.

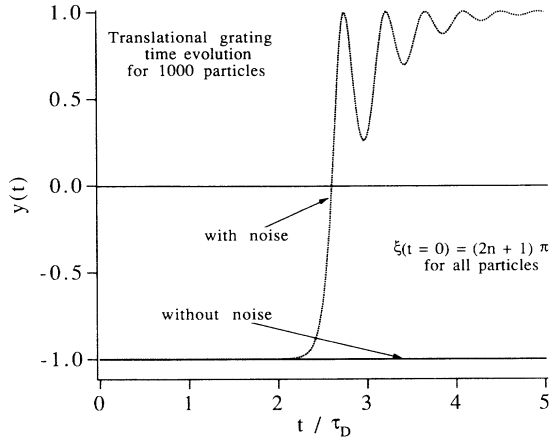

FIG. 9. Formation of a translational index grating out of noise arising from thermal fluctuations.

tially at rest and placed randomly on the plane. Thus $n(\xi,0)$ is a random function of ξ, so that the grating function is initially zero. An examination of this figure reveals that $y(t)$ evolves smoothly, on a time scale set by τ_D and saturates to its peak value of unity corresponding to the spheres all occupying the positions where the electrostrictive potential is a minimum.

2. *Evolution of the grating in the underdamped case*

Next we examine the underdamped case, which is depicted in Fig. 8 for 1000 spherical, 100-μm-sized metal particles, irradiated by 0.5-W/cm^2 microwave beams. The grating spacing is taken to be 1 mm and the mass density of the spheres $\rho=0.1$ g/cm^3. For these conditions any individual particle will undergo several oscillations about the equilibrium position, as depicted in Fig. 3. However, a collection of particles placed at different points will make contributions to the grating function $y(t)$ that are somewhat out of phase with one another,

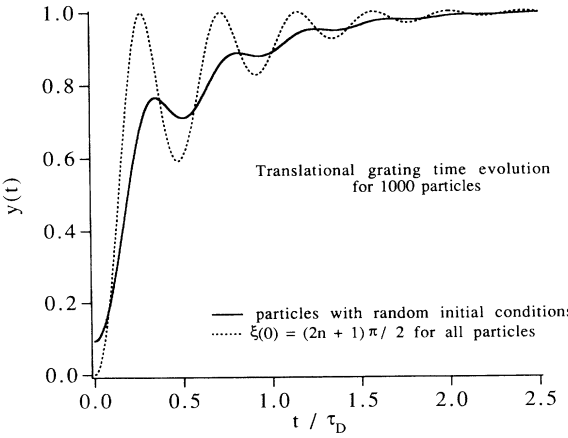

FIG. 8. Formation of a translational index grating in the underdamped case for two situations: (i) the spheres randomly placed initially, and (ii) the spheres are all placed at points where the electrostrictive force is a maximum.

and this will tend to reduce these oscillations. Two different physical situations are considered: (i) the particles are initially randomly distributed at rest (solid line), and (ii) all of the particles are placed at the points where the electrostrictive force is most repulsive, i.e., $\xi=(2n+1)\pi/2$ (dotted line). An examination of Fig. 9 reveals that the first case has only weak oscillations, reflecting the fact that the motions of the particles are not in phase with one another. Note that in both cases the grating function achieves a value of nearly unity by a time of τ_D.

3. *Evolution of the grating due to noise*

In this section we examine the role of thermal fluctuations in grating formation. Thermodynamic fluctuations are important in the transient evolution of the translation optical index grating for the situation in which the spheres are all initially at rest and positioned at points of unstable equilibrium, i.e., if the particles are all positioned at the points $\xi(0)=(2n+1)\pi$, where the electrostrictive force is zero. In the absence of Langevin forces, the spheres are not subject to any forces at all, and they will remain at the points of unstable equilibrium and $y(t)=-1$, for all time.

Now the points $\xi(0)=(2n+1)\pi$ are points of unstable equilibrium, and if the particles are just slightly displaced away from them, the electrostrictive force will tend to push them further away and the sphere density will begin to evolve towards a true Maxwell-Boltzmann distribution. Once this has occurred, a translational index grating will begin to form with $y(t)\rightarrow+1$.

The dotted curve in Fig. 9 depicts the transient behavior of the translational index grating as it evolves from this unstable equilibrium value under the influence of first Langevin and then electrostrictive forces. An examination of the figure reveals that it takes a time on the order of $2\tau_D$ for thermodynamic fluctuations to push the spheres far enough away from their initial points for electrostrictive forces to dominate their motion and reorder

them into their steady-state positions of true equilibrium, where $y(t)$ is nearly unity. The figure depicts the underdamped case with the same system parameters used in Fig. 8.

C. Index grating formation: Planck-Nernst approach

Next we compare the Monte Carlo calculations discussed above with the solutions one obtains from the Planck-Nernst equation. More precisely, we solve the Planck-Nernst equation for the evolution of the particle density irradiated by two degenerate, plane-wave cw beams. We find that the predictions of these two approaches are the same, provided they have the same physical parameters.

The Planck-Nernst equation for the transient dynamics of a collection of spherical particles in a viscous fluid irradiated by a static electromagnetic interference pattern is [5]

$$\frac{\partial n}{\partial t}=D\nabla\cdot\left[\nabla n+n\frac{\nabla U}{kT}\right], \tag{4.2}$$

where U is the electrostrictive potential given in Eq. (2.13). Figure 10 compares the time evolution of the grating function generated by the Monte Carlo approach $[y_{\rm MC}(t)]$ and the Planck-Nernst equation $[y_{\rm PN}(t)]$. The specific situation modeled is one in which the array is in the overdamped regime with the same system parameters as were used in Figs. 5 and 6. An examination of this figure reveals that $y_{\rm MC}(t)$ and $y_{\rm PN}(t)$ are virtually the same, as one would expect on physical grounds. The small differences between $y_{\rm MC}(t)$ and $y_{\rm PN}(t)$ that do appear arise from the fact that the Monte Carlo treatment involved only 1000 particles, whereas the Planck-Nernst equation assumes a continuous distribution of spheres.

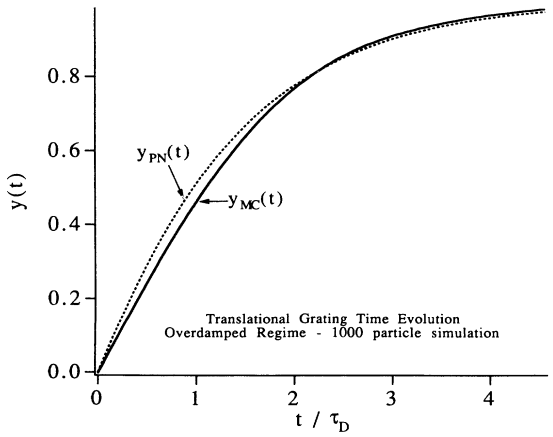

FIG. 10. Time evolution of the grating function for the array $y(t)$ vs time from the Monte Carlo simulations and solutions of the Planck-Nernst equation.

V. FOUR-WAVE MIXING IN TRANSLATIONAL OPTOMECHANICAL MEDIA

In this section we examine optical phase conjugation, pump grating modulation, and harmonic phase conjugation with a three-dimensional array of electrically isotropic spheres as the active medium. We will once again confine ourselves to situations in which the polarization of the incident radiation beams are confined to lie in the plane of the particles. Since the particles cannot respond to radiation polarized perpendicular to their support planes, the optical response of the array is isotropic only within the plane of the particles. Overall, the nonlinear-optical response is quite anisotropic.

Let $\mathbf{E}(\mathbf{r},t)$ be the total electric field of the incident radiation fields:

$$\mathbf{E}(\mathbf{r},t)=E_0\sum_{m=1,2,p,p_c}\mathbf{e}_m b_m\exp[i(\mathbf{K}_m\cdot\mathbf{r}-\omega_m t)]+\text{c.c.}\ , \tag{5.1}$$

with $\mathbf{e}_m$, $E_m\equiv E_0 b_m$, $\mathbf{K}_m$, and ω_m are the unit polarization vector, complex amplitude, propagation vector, and frequency of the mth beam, respectively. Here $m=1$ (2) corresponds to the pump beam propagating to the right (left), $m=p$ refers to the probe wave, and $m=p_c$ corresponds to the wave that is phase conjugate to the probe. For standard phase conjugation, $\mathbf{K}_1=-\mathbf{K}_2\equiv\mathbf{K}$; $\mathbf{K}_p=-\mathbf{K}_{pc}\equiv\mathbf{Q}$, and all of the frequencies are degenerate, i.e., $\omega_m\equiv\omega$. In this paper we shall work within the nondepleted pump regime and assume equal pumps. Thus, we take $b_1=b_2=1$.

In harmonic phase conjugation [11], one pump wave (e.g., $m=1$) and the signal beam are degenerate and act as write beams to form the static optical index gratings. If the medium is sufficiently nonlinear, notable higher-order index gratings will form whose spatial wave vectors are integral multiples of the fundamental, first-order grating. If the frequency of the counterpropagating ($m=2$) pump beam is a harmonic of the signal wave (we are assuming that the medium is nondispersive, an excellent approximation since it is mostly air), then it will act as a read beam and be Bragg diffracted by the appropriate higher-order index grating to form a beam whose phase is conjugate to the initial probe wave. Note that the frequency of this wave is the same as that of the read beam, although its direction of propagation is opposite to that of the signal wave. As a specific example, suppose that the frequency of the read beam is equal to the third harmonic of the write beams, e.g., $\omega_1=\omega_p=\omega$ and $\omega_2=3\omega$. Then a phase conjugate wave that is the third harmonic of the signal wave will be generated.

A. Phase conjugation in translational optomechanical media

The phase conjugate characteristics of an isotropic optomechanical medium are set by the nonlinear polarization vector. $\mathbf{P}_{\rm NL}^{(c)}(\mathbf{r},t)$, which gives rise to the conjugate beam. $\mathbf{P}_{\rm NL}^{(c)}(\mathbf{r},t)$ arises from optical index gratings created by the signal with either pump beam. In addition, a grat-

ing is created by the two pump waves, and this grating can give rise indirectly to additional contributions to the phase conjugation process.

To see why these three index gratings are important, we note that in the absence of a phase conjugate beam the electrostrictive potential can be written as

$$\frac{U(\mathbf{r})}{k\mathbf{T}} = -g\{b_S \mathbf{e}_1\cdot\mathbf{e}_p\cos[(\mathbf{K}-\mathbf{Q})\cdot\mathbf{r}] + b_S\mathbf{e}_1\cdot\mathbf{e}_p\cos[(\mathbf{K}+\mathbf{Q})\cdot\mathbf{r}] + \mathbf{e}_1\cdot\mathbf{e}_2\cos(2\mathbf{K}\cdot\mathbf{r})\}\ , \tag{5.2}$$

where $g\equiv\alpha E_0^2/4kT$. Examination of Eq. (5.2) reveals the desired density gratings. Since all of the beams are degenerate the equilibrium sphere density is given by the Maxwell-Boltzmann distribution. If the phase conjugate beam is sufficiently weak, we can to a first approximation neglect any grating formed by the conjugate beam in concert with either pump wave. Then the density of particles $n(\mathbf{r})$ is given by

$$n(\mathbf{r}) = \frac{n_0\exp\left[\dfrac{U(\mathbf{r})}{kT}\right]}{I_0(g\mathbf{e}_S\cdot\mathbf{e}_1 b_S)I_0(g\mathbf{e}_S\cdot\mathbf{e}_2 b_S)I_0(g\mathbf{e}_2\cdot\mathbf{e}_1)}\ . \tag{5.3}$$

Expanding $n(\mathbf{r})$ into grating orders, we have

$$n(\mathbf{r}) = \sum_{k=0}^{\infty}\sum_{l=0}^{\infty}\sum_{m=0}^{\infty}\Delta_{klm}n_{klm}M_{klm}(\mathbf{r})\ , \tag{5.4a}$$

$$M_{klm}(\mathbf{r}) = \cos[k(\mathbf{K}-\mathbf{Q})\cdot\mathbf{r}]\cos[l(\mathbf{K}+\mathbf{Q})\cdot\mathbf{r}] \times\cos[2m\mathbf{K}\cdot\mathbf{r}]\ , \tag{5.4b}$$

$$\Delta_{klm} \equiv (2-\delta_{k,0})(2-\delta_{l,0})(2-\delta_{m,0})\ , \tag{5.4c}$$

$$n_{klm} \equiv n_0\frac{I_k(g\mathbf{e}_S\cdot\mathbf{e}_1 b_S)I_l(g\mathbf{e}_S\cdot\mathbf{e}_2 b_S)I_m(g\mathbf{e}_2\cdot\mathbf{e}_1)}{I_0(g\mathbf{e}_S\cdot\mathbf{e}_1 b_S)I_0(g\mathbf{e}_S\cdot\mathbf{e}_2 b_S)I_0(g\mathbf{e}_2\cdot\mathbf{e}_1)}\ . \tag{5.4d}$$

An examination for Eq. (5.4d) reveals that three different types of optical index gratings can be created by the signal beam and the two counterpropagating pump waves. These are the signal with either pump, which create index grating with wave vectors of the form $k(\mathbf{K}+\mathbf{Q})$ and $l(\mathbf{K}-\mathbf{Q})$. The two pump beams form grating with wave vectors $2m\mathbf{K}$.

Note that if the conjugate beam attains any intensity, then it is necessary to include effects arising from the formation of optical index gratings between the phase conjugate wave and either pump beam as well as the gratings formed by the conjugate beam and the probe wave. Generally speaking, the latter are usually much weaker than the other beams and will be neglected. To further simplify matters we will also always work within the nondepleted pump approximation (which is consistent with dropping the gratings formed by the signal and conjugate waves). Writing the conjugate wave amplitude and polarization as $\mathbf{e}_{pc}$ and b_{pc}, we have

$$\frac{U(\mathbf{r})}{kT} = -g\{b_s\mathbf{e}_1\cdot\mathbf{e}_S\cos[(\mathbf{K}-\mathbf{Q})\cdot\mathbf{r}]+b_S\mathbf{e}_1\cdot\mathbf{e}_S\cos[(\mathbf{K}+\mathbf{Q})\cdot\mathbf{r}]\} - g\{b_{pc}\mathbf{e}_1\cdot\mathbf{e}_{pc}\cos[(\mathbf{K}+\mathbf{Q})\cdot\mathbf{r}]+b_{pc}\mathbf{e}_1\cdot\mathbf{e}_{pc}\cos[(\mathbf{K}-\mathbf{Q})\cdot\mathbf{r}]\} - g\mathbf{e}_1\cdot\mathbf{e}_2\cos(2\mathbf{K}\cdot\mathbf{r})\ , \tag{5.5}$$

and the particle density is

$$n(\mathbf{r}) = \frac{n_0\exp\left[\dfrac{U(\mathbf{r})}{kT}\right]}{I_0[g(\mathbf{e}_S\cdot\mathbf{e}_1 b_S+\mathbf{e}_{pc}\cdot\mathbf{e}_2 b_{pc})]I_0[g(\mathbf{e}_S\cdot\mathbf{e}_2\mathbf{b}_S+\mathbf{e}_{pc}\cdot\mathbf{e}_1 b_{pc})]I_0(g\mathbf{e}_2\cdot\mathbf{e}_1)}\ . \tag{5.6}$$

Expanding $n(\mathbf{r})$ into grating orders, we have

$$n(\mathbf{r}) = \sum_{k=0}^{\infty}\sum_{l=0}^{\infty}\sum_{m=0}^{\infty}\Delta_{klm}n_{klm}\mathcal{M}_{lkm}(\mathbf{r})\ , \tag{5.7a}$$

$$\mathcal{M}_{klm}(\mathbf{r}) = \cos[k(\mathbf{K}-\mathbf{Q})\cdot\mathbf{r}]\cos[l(\mathbf{K}+\mathbf{Q})\cdot\mathbf{r}]\cos(2m\mathbf{K}\cdot\mathbf{r})\ , \tag{5.7b}$$

$$\Delta_{klm} \equiv (2-\delta_{k,0})(2-\delta_{1,0})(2-\delta_{m,0})\ , \tag{5.7c}$$

$$\frac{n_{lkm}}{n_0} \equiv \frac{I_k[g(\mathbf{e}_S\cdot\mathbf{e}_1 b_S+\mathbf{e}_{pc}\cdot\mathbf{e}_2 b_{pc})]I_1[g(\mathbf{e}_S\cdot\mathbf{e}_2 b_s+\mathbf{e}_{pc}\cdot\mathbf{e}_1 b_{pc})]I_m(g\mathbf{e}_2\cdot\mathbf{e}_1)}{I_0[g[\mathbf{e}_S\cdot\mathbf{e}_1 b_S+\mathbf{e}_{pc}\cdot\mathbf{e}_2 b_{pc})]I_0[g(\mathbf{e}_S\cdot\mathbf{e}_2 b_S+\mathbf{e}_{pc}\cdot\mathbf{e}_1 b_{pc})]I_0(g\mathbf{e}_2\cdot\mathbf{e}_1)}\ . \tag{5.7d}$$

The simplest case occurs when the counterpropagating pump beams are orthogonally polarized and g is either very large or very small. We shall treat this case first.

1. Phase conjugation: Orthogonality polarized pump beams

For this case only the first-order gratings with spatial periods of $\mathbf{K}\pm\mathbf{Q}$ will diffract either pump beam into the appropriate direction and form a beam that is phase conjugate to the signal. Examination of Eqs. (5.4) reveals that the grating components n_{100} and n_{010} contribute directly. In particular, the portion of the particle density of interest can be written as

$$\delta n(\mathbf{r}) = \mathbf{n}_{100}\cos[(\mathbf{K}-\mathbf{Q})\cdot\mathbf{r}]+n_{010}\cos[(\mathbf{K}+\mathbf{Q})\cdot\mathbf{r}]\ . \tag{5.8}$$

To simplify matters, we shall assume that the signal beam is polarized parallel to the first pump beam. Then the phase conjugate wave will be polarized parallel to the second pump beam and the nonlinear polarization that generates the phase conjugate beam is $\mathbf{P}(\mathbf{r},t)=\Pi\exp[i(\mathbf{Q}\cdot\mathbf{r}-\omega t)]+\text{c.c.}$, where

$$\Pi(\mathbf{r},t)=\alpha E_0\left[\frac{\mathbf{I}_1(g\mathbf{e}_S\cdot\mathbf{e}_1 b_S)}{\mathbf{I}_0(g\mathbf{e}_S\cdot\mathbf{e}_1 b_S)}\mathbf{e}_2\right] . \tag{5.9a}$$

The nonlinear polarization that amplifies the signal beam is equal to $\mathbf{P}(\mathbf{r},t)=\Pi\exp[i(\mathbf{Q}\cdot\mathbf{r}+\omega t)]+\text{c.c.}$:

$$\Pi(\mathbf{r},t)=\alpha E_0\left[\frac{\mathbf{I}_1(g\mathbf{e}_{pc}\cdot\mathbf{e}_2 b_{pc})}{\mathbf{I}_0(g\mathbf{e}_{pc}\cdot\mathbf{e}_2 b_{pc})}\mathbf{e}_1\right] . \tag{5.9b}$$

Inserting Eqs. (5.9) into the Maxwell equations and making the slowly varying envelope approximation, we obtain the following coupled wave equations for the conjugate and signal waves:

$$\frac{\partial b_{pc}}{\partial z}=-2i\pi Q\alpha n_0\frac{\mathbf{I}_1(gb_S)}{\mathbf{I}_0(gb_S)} , \tag{5.10a}$$

$$\frac{\partial b_S}{\partial z}=-2i\pi Q\alpha n_0\frac{\mathbf{I}_1(gb_{pc})}{\mathbf{I}_0(gb_{pc})} . \tag{5.10b}$$

In the limit that $g\ll 1$, we can expand the Bessel functions in powers of g and solve for the emitted conjugate and amplified probe waves. In particular, we find that the four-wave-mixing coefficient for in this limit is $\kappa=\pi Q\alpha n_0(\alpha E_0^2/kT)$. For metal particles, this can be written as $\kappa=3\pi Qf(\alpha I_{\text{pump}}/ckT)$. If $\kappa L\ll 1$, $I_{pc}\propto I_{\text{pump}}^2 I_S(0)$. For large g the grating should saturate and

$$I_{pc}(g)\rightarrow 2.25(fQL)^2 I_{\text{pump}} , \tag{5.11}$$

which is a saturated intensity.

2. *Phase conjugation: parallel polarized pump beams, pump grating modulation*

If the pump beams are polarized parallel to one another, then index gratings with grating vectors $2m\mathbf{K}$ will be induced in the medium. Furthermore, the first-order pump grating wave vector $2\mathbf{K}$, can modulate the $\mathbf{K}\pm\mathbf{Q}$ gratings to produce additional index gratings. This process is referred to as pump beam modulation [11] and it can act to either enhance or reduce the phase conjugate reflectivity. Specifically, the pump grating couples with the first-order $\mathbf{K}+\mathbf{Q}$ grating to produce a $\mathbf{K}-\mathbf{Q}$ grating. It also couples with the first-order $\mathbf{K}-\mathbf{Q}$ grating to produce a contribution to the $\mathbf{K}+\mathbf{Q}$ grating. Thus the grating components n_{101} and n_{011} will also contribute. The portion of the sphere density of interest to phase conjugate, $\delta n(\mathbf{r})$, is

$$\delta n(\mathbf{r})=(n_{100}+n_{011})\cos[(\mathbf{K}-\mathbf{Q})\cdot\mathbf{r}]+(n_{001}+n_{110})\cos[(\mathbf{K}+\mathbf{Q})\cdot\mathbf{r}] . \tag{5.12}$$

The polarization of the medium $\mathbf{P}(\mathbf{r},t)\equiv\alpha n(\mathbf{r})\mathbf{E}(\mathbf{r},t)$ and the portion responsible for generating a phase conjugate beam is $\mathbf{P}(\mathbf{r},t)=\Pi\exp[i(\mathbf{Q}\cdot\mathbf{r}-\omega t)]+\text{c.c.}$, with $\Pi=\Pi_1+\Pi_2$, where

$$\Pi_1(\mathbf{r},t)=n_0\alpha E_0\left[\frac{\mathbf{I}_1(g\mathbf{e}_S\cdot\mathbf{e}_1 b_S)}{\mathbf{I}_0(g\mathbf{e}_S\cdot\mathbf{e}_1 b_S)}+\frac{\mathbf{I}_1(g\mathbf{e}_S\mathbf{e}_2 b_S)\mathbf{I}_1(g\mathbf{e}_2\cdot\mathbf{e}_1)}{\mathbf{I}_0(g\mathbf{e}_S\cdot\mathbf{e}_2 b_S)\mathbf{I}_0(g\mathbf{e}_2\cdot\mathbf{e}_1)}\right]\mathbf{e}_1 \tag{5.13a}$$

and

$$\Pi_2(\mathbf{r},t)=n_0\alpha E_0\left[\frac{\mathbf{I}_1(g\mathbf{e}_S\cdot\mathbf{e}_2 b_S)}{\mathbf{I}_0(g\mathbf{e}_S\cdot\mathbf{e}_2 b_S)}+\frac{\mathbf{I}_1(g\mathbf{e}_S\cdot\mathbf{e}_1 b_S)\mathbf{I}_1(g\mathbf{e}_2\cdot\mathbf{e}_1)}{\mathbf{I}_0(g\mathbf{e}_S\cdot\mathbf{e}_1 b_S)\mathbf{I}_0(g\mathbf{e}_2\cdot\mathbf{e}_1)}\right]\mathbf{e}_2 . \tag{5.13b}$$

The first and third terms in Eqs. (5.14) are the standard saturated forms for an artificial Kerr medium. The second and fourth terms arise from pump grating modulation and represent the effect of strong pump gratings. To determine the phase conjugate reflectively, we insert $\mathbf{P}(\mathbf{r},t)$ into the Maxwell equations, make the slowly varying envelope approximation (SVEA) and solve for the conjugate wave.

There are several cases that are worth considering. If all of the beams are linearly polarized in the same direction, then

$$\mathbf{P}(\mathbf{r},t)=2\alpha n_0 E_0\left[\frac{\mathbf{I}_1(gb_S)}{\mathbf{I}_0(gb_S)}+\frac{\mathbf{I}_1(gb_S)\mathbf{I}_1(g)}{\mathbf{I}_0(gb_S)\mathbf{I}_0(g)}\right]\times\exp[i(\mathbf{K}_{pc}\cdot\mathbf{r}-\omega t)]+\text{c.c.} , \tag{5.14}$$

and the conjugate intensity $I_{pc}(0)$ in the small signal is

$$I_{pc}(g)=2.25(fQL)^2\times\left[\frac{\mathbf{I}_1(gb_S)}{\mathbf{I}_0(gb_S)}+\frac{\mathbf{I}_1(gb_S)\mathbf{I}_1(g)}{\mathbf{I}_0(gb_S)\mathbf{I}_0(g)}\right]^2 I_{\text{pump}} , \tag{5.15}$$

where f is the volume fraction of spheres and I_{pump} is the pump intensity. Examination of Eq. (5.15) reveals that in the limit that $g\rightarrow 0$, $I_{pc}\propto I_{\text{pump}}^2 I_S(0)$ as expected. However, for $|g|\gg 1$ and g positive, the phase conjugate beam is independent of the probe power, directly proportional to the pump intensity, and is volume fraction limited. This is a saturated regime and is valid as long as $gb_S\gg 1$, which can involve very low probe wave intensities if the particles are large enough. For example, for 100-μm-sized metal spheres with $I_{\text{pump}}=1$ W/cm^2, $g=(\pi/3)10^5(I_{\text{beam}})^{1/2}$. If probe intensity is on the order of 1 μW/cm^2, the system will operate in the saturated regime.

If g is negative, then we can rewrite Eq. (5.16) as

$$I_{pc}(g)=2.25(fQL)^2\left[\frac{\mathbf{I}_1(gb_S)}{\mathbf{I}_0(gb_S)}\right]^2\left[1-\frac{\mathbf{I}_1(g)}{\mathbf{I}_0(g)}\right]^2 I_{\text{pump}} , \tag{5.16}$$

which in the limit of large $|g|$, $I_{pc}\rightarrow(2.25/4)I_{\text{pump}}(fQL/g)^2$. Thus the emitted conjugate

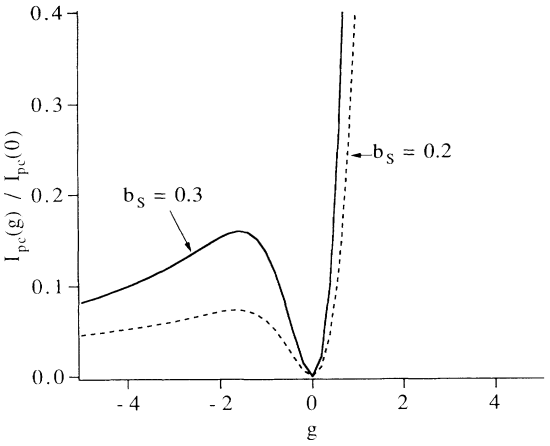

FIG. 11. $I_{pc}(g)/I_{pc}(0)$ vs g for $b_S=0.2$ and 0.3.

wave scales inversely with I_{pump} and is independent of probe intensity, i.e., $I_{pc}\rightarrow 1/I_{\text{pump}}$. These features of optomechanical electrodynamics are clearly seen in Fig. 11, which depicts the phase conjugate intensity versus pump intensity for two different probe intensities.

Finally, we comment on the onset of pump depletion. Generally speaking, pump depletion is an issue whenever the phase conjugate intensity grows to a finite fraction of the pump power and in the saturated regime, $I_{pc}\rightarrow 2.25(fQL)^2 I_{\text{pump}}$, for $gb_S \gg 1$. Thus pump depletion is an issue for situations in which $fQL \geq 0.2$.

B. Harmonic phase conjugation

We consider the situation in which the first pump beam and the probe wave have the same frequency ω and the second pump is the kth harmonic of this, i.e., $k\omega$. Then the strength of the grating of interest is $n_k(gb_S)=n_0 I_k(gb_S)/I_0(gb_S)$, where

$$gb_S \equiv \alpha(\mathbf{e}_1\cdot\mathbf{e}_S)E_0^2 b_S/2kT$$

and b_S is the ratio of the probe electric-field amplitude to that of the first pump. It follows that if the second pump beam, which is oscillating at the frequency $k\omega$, has an electric-field vector of $\mathbf{e}_k E_k \exp[ik(\mathbf{K}\cdot\mathbf{r}-\omega t)]$, then the nonlinear polarization responsible for generating the harmonic phase conjugate radiation of order k is

$$\mathbf{P}_{pc}^{(k)}(\mathbf{r},t)=n_0\alpha[I_k(gb_S)/I_0(gb_S)]\mathbf{e}_k \times E_k \exp[ik(\mathbf{Q}\cdot\mathbf{r}+\omega t)]+\text{c.c.} \quad (5.17)$$

Note that the magnitude of this polarization is independent of grating order in the limit that $g \gg 1$.

Next we examine the emitted harmonic phase conjugate beam. Since the index gratings set up by the signal and first pump beam are static, no energy is transferred from them to either the second pump beam or the conjugate wave, which are oscillating at the kth harmonic. Furthermore, the signal and first pump beam will not exchange energy with each other. However, the harmonic phase conjugate beam is formed by Bragg scattering of the second pump beam by the kth index grating. If enough energy is diffracted from the second pump beam, then depletion will occur and it will be necessary to include this effect as well. Thus we require coupled equations for the second pump beam and the harmonic phase conjugate wave and require the nonlinear polarization $\mathbf{P}_2^{(k)}(\mathbf{r},t)$ that diffracts the harmonic phase conjugate beam into the second pump wave. Since this uses the same index grating, it is

$$\mathbf{P}_2^{(k)}(\mathbf{r},t)=n_0\alpha[I_k(gb_S)/I_0(gb_S)]\mathbf{e}_{pc}^{(k)}E_{pc}^{(k)} \times \exp[iK(\mathbf{Q}\cdot\mathbf{r}+\omega t)]+\text{c.c.}\ , \quad (5.18)$$

where $\mathbf{e}_{pc}^{(k)}E_{pc}^{(k)}\exp[ik(\mathbf{Q}\cdot\mathbf{r}+\omega t)]$ is the harmonic phase conjugate electric field. The coupled wave equations for the harmonic phase conjugate beam and the second pump beam are

$$2ik\mathbf{Q}\cdot\nabla\mathbf{E}_{pc}^{k}=-4\pi(kQ)^2\alpha n_0\frac{I_k(gb_S)}{I_0(gb_S)}E_k\ , \quad (5.19a)$$

$$2ik\mathbf{K}\cdot\nabla E_k=-4\pi(kQ)^2\alpha n_0\frac{I_k(gb_S)}{I_0(gb_S)}\mathbf{E}_{pc}^{k}\ . \quad (5.19b)$$

Thus the basic length scale for generating harmonic phase conjugate waves of order k is $\kappa_k(k\omega)=2\pi kQ\alpha n_0 I_k(gb_S)/I_0(gb_S)$. If the optical pathlength is L and the two beams are nearly collinear, the intensity of the kth-harmonic phase conjugate wave is

$$I_{pc}^{(k)}=I_2(0)\sin^2\kappa_k(k\omega)L\ . \quad (5.20)$$

Figure 12 depicts the intensity of the second-harmonic conjugate beam and the pump wave (normalized to the second pump beam's initial intensity) as a function of g for the case in which $b_S=1$, $f=0.01$, $\lambda=3$ cm, and $L=50$ cm. An examination of this figure reveals that significant diffraction of the second pump or read beam and creation of the second harmonic phase conjugate radiation occurs by $g=2$. For 10-μm-sized metallic spheres, this occurs when the rms product of the writing beam intensities is 19 mW/cm^2. For large values of the beam intensities, $\kappa_k L$ continues to increase and the pump

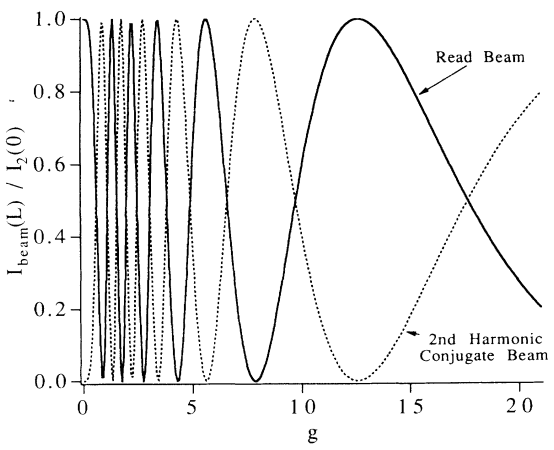

FIG. 12. Intensity of the second-harmonic conjugate beam and the pump wave as a function of g for the case in which $b_S=1$, $f=0.1$, $\lambda=3$ cm, and $L=50$ cm.

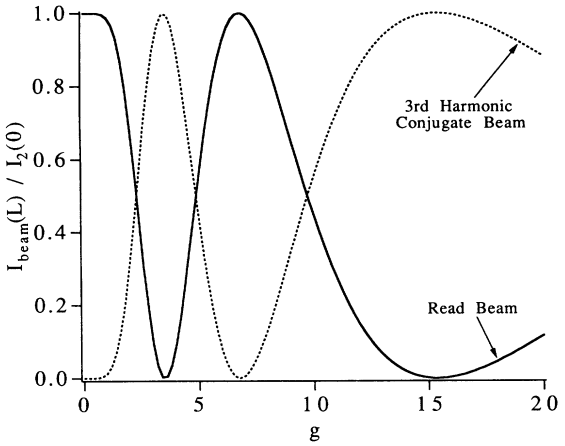

FIG. 13. Intensity of the third-harmonic conjugate beam and the pump wave as a function of g for the case in which $b_S=1$, $f=0.1$, $\lambda=3$ cm, and $L=50$ cm.

is significantly depleted. Thereafter, further increases in writing beam intensities causes a periodic interchange of energy between the read beam and the harmonic phase conjugate wave. Eventually, further increases in writing beam intensities saturates the mixing coefficient and there are no further changes in the beam intensities.

Figure 13 depicts the intensity of the third-harmonic conjugate beam and the pump wave (normalized to the second pump beam's initial intensity) as a function of g again for the case in which $b_S=1$, $f=0.01$, $\lambda=3$ cm, and $L=50$ cm. An examination of this figure reveals that significant diffraction of the second pump or read beam and creation of the third-harmonic phase conjugate radiation occurs by $g=3$. For 10-μm-sized metallic spheres, this occurs when the rms product of the writing beam intensities is 28.5 W/cm^2. Note that the beam intensities undergo fewer oscillations because generation of higher-order index gratings tends to require more intense write beams and this in turn translates into the requirement for larger values of g. Finally, Fig. 14 depicts the intensity of

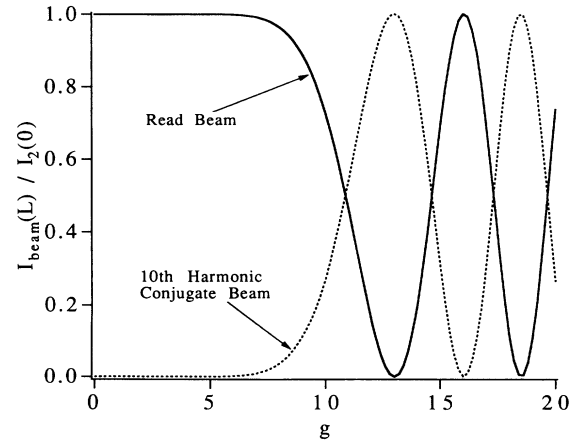

FIG. 14. Intensity of the tenth-harmonic conjugate beam and the pump wave as a function of g for the case in which $b_S=1$, $f=0.1$, $\lambda=3$ cm, and $L=50$ cm.

the tenth-harmonic conjugate beam and the pump wave (normalized to the second pump beam's initial intensity) as a function of g again for the case in which $b_S=1$, $f=0.01$, $\lambda=3$ cm, and $L=50$ cm. An examination of this figure reveals that significant diffraction of the second pump or read beam and creation of the third-harmonic phase conjugate radiation occurs by $g=10$. For 10-μm-sized metallic spheres, this occurs when the rms product of the writing beam intensities is 190 mW/cm^2. Note that the beam intensities undergo even fewer oscillations than the third-harmonic case and the general trends established for the lower-order gratings continue.

For $L/\lambda\approx 50$, $f\approx 10^{-2}$ is required. For 10-μm spheres, this implies $n_0=10^7$ particles/cm^3. For 94-GHz radiation the required system size is on the order of 50 cm, implying $N=1.2\times 10^{12}$.

VI. DISCUSSION AND CONCLUSIONS

In this paper we have examined the mechanical, dielectric, and nonlinear-optical response of a translational optomechanical medium to electromagnetic radiation. The specific medium considered consists of a three-dimensional array of dielectric or metal spheres that are mechanically supported but free to roll on a set of transparent, very thin planes. Such media are of interest for active optical processes such as wave-mixing applications in the submillimeter, millimeter, and microwave regions of the electromagnetic spectrum.

The strong dielectric response of translational optomechanical media to long-wavelength radiation makes them an interesting class of candidates for active media at these wavelengths. As discussed in this paper, it is very difficult to extend four-wave-mixing processes to microwave or millimeter wavelengths due to the problems associated with beam intensities and the scaling properties of the nonlinear susceptibilities. Specifically, the four-wave-mixing coefficient for optical Kerr media scales with wavelength as λ^{-3}. Thus κL declines by some nine orders of magnitude if one attempts to scale from visible to millimeter wavelengths, unless materials with unusually large nonlinear susceptibilities are available.

In the unsaturated regime, $\chi^{(3)}$ for artificial Kerr media scale as the particle volume for a fixed volume fraction of spheres Thus this nine-orders-of-magnitude deficiency can be overcome by scaling up the particle sizes from tenths of a μm to tens of μm. For 10-μm-sized metal spheres, such as aluminum or copper, the electrical polarizability $\alpha\rightarrow 10^{-9}$ cm^3, whereas for 100-μm-sized spheres, $\alpha\rightarrow 10^{-6}$ cm^3. If the pump power is 1 mW/cm^2 and the signal power is 1 nW/cm^2, the medium will operate in the unsaturated regime and $\chi^{(3)}\rightarrow 3\pi f r_0^3 I_{\text{pump}}/ckT$, which for $f=10^{-4}$ can be on the order of 7.85×10^{-3} esu. Thus these media exhibit a very strong dielectric response even at low beam powers.

For these materials, saturation is governed by a dimensionless parameter g, which is essentially the ratio of the electrostrictive energy arising from the interaction of a given sphere with both the pump and signal beams to the

thermal energy per particle. For 100-μm-sized metallic or metal-coated spheres at room temperatures, $g \approx (I_p I_s)^{1/2} 10^5$, so that the medium is saturated even with mW/cm^2 pump and signal beams. Once the medium is saturated, the size of the nonlinear susceptibility $\chi^{(3)} \rightarrow 3f/4\pi$, i.e., it is volume fraction limited. If the volume fraction is 10^{-4}, then the third-order optical susceptibility approaches 2.39×10^{-5} esu. This is very large and ensures efficient phase conjugation even at these incredibility low beam powers.

Another feature of translational optomechanical media that is of interest is the fact that due to the very deep index gratings that they form in response to moderate radiation intensities, a variety of novel saturation effects are expected to manifest themselves. For example, for the saturation case mentioned above, very high-order index gratings are readily formed. Specifically, index gratings of order $k \approx g$ should be excited in an optomechanical array by incident radiation.

We investigated the dynamics of individual spheres rolling on a plane from the perspective of the Langevin equations. Examination of the equations of motion revealed three different dynamic regimes for these particles. Specifically, (i) a diffusive regime, (ii) an overdamped regime, and (iii) and underdamped regime. Thermal fluctuations will dominate the particle's motion if the electrostrictive force is less than the Langevin force, i.e., $U \ll kT$. This regime is characteristic of suspension dynamics and only for the very smallest particles is stochastic behavior of any consequence. For example, with 40-μm-sized spheres, stochastic motion typically occurs on a spatial scale set by several tens of Å. For 1-μm-sized spheres, the spatial scale is on the order of the particle size. This behavior is to be expected since $\Gamma(t)$ increases rapidly with decreasing particle size.

The particle is in the overdamped regime if $\eta(1/I_{\text{beam}}\rho)^{1/2} \gg (r_0^2 K)$ and the response time $\tau_R \equiv Q^2(15 r_0^2 I_{\text{beam}}/39\eta c)$. This can be rewritten as $\tau_R^{-1} \approx D' K^2 (U/kT)$, with $D' = 15kT/156\pi\eta r_0$ the translational diffusion coefficient for a sphere moving in a medium with a viscosity η. This should be contrasted with suspensions in the driven regime, where the medium response time $\tau_R^{-1} = DK^2(U/k_B T)$, with $D = 6\pi kT/r_0\eta$ being the diffusion coefficient for a sphere in a viscous fluid. Finally, if $\eta(1/I_{\text{beam}}\rho)^{1/2} \ll (r_0^2 K)$, the particle motion is underdamped. Here the particle motion is characterized by oscillations, of frequency ω_0, about the equilibrium points that decay in amplitude on a time scale set by β^{-1}.

These results imply that the optical response time of the medium in the overdamped regime scales as $\eta(\Lambda/r_0)^2 (I_1 I_p)^{-1/2}$. This should be contrasted with a liquid suspension of microspheres in the diffusive regime where the optical response time scales as $\eta\Lambda^2 r_0/kT$. Accordingly, by using 100-μm-sized spheres as opposed to 1000-Å polystyrene spheres, the medium response is reduced by a factor of 10^4. Furthermore, the viscosity of air at normal atmospheric pressure and temperature is two orders of magnitude smaller than water. Thus, despite the fact that Λ for microwaves is four to five orders of magnitude greater than in Askhin's experiments at argon-ion wavelengths, we anticipate that the medium response time will be shorter with optomechanical media than for 1000-Å polystyrene spheres. If the beam intensity is increased so that the system is in the underdamped regime, it is possible to further reduce the medium response time. In this regime, the optical response time is set by $1/\beta \approx r_0^2/\eta$. Thus, greater reductions can be achieved with large particles.

Our dynamic calculations focused on solving the differential equations for the motion of a single sphere under the action of electrostrictive forces, friction, reaction forces from contact with the surface, and Langevin forces associated with thermal fluctuations. The transient behavior of the array was obtained by summing over the motion of each individual sphere which was initially at rest and randomly placed. Calculations indicated that the array evolved to a steady-state distribution that was dictated by Maxwell-Boltzmann statistics. Furthermore, in the overdamped regime, direct comparison with the Planck-Nernst equation showed that the array behaved just as a suspension with the same system parameters of viscosity, laser intensity, dielectric properties, and sphere size.

In the underdamped regime, the evolution of the array density displayed transient oscillations, reflecting the motion of individual spheres that oscillated about the equilibrium point. In this regime the array achieved steady state on a time scale set by β^{-1}. There does not appear to be a direct analog to suspension dynamics in this case, as there are no dynamical equations that are generally applicable for underdamped motion.

One of our numerical simulations did find a significant role for thermodynamic fluctuations, as manifested in the Langevin noise term in the dynamical behavior of isotropic optomechanical media. Specifically, if the array is initially prepared in a state in which all of the particles are initially at rest and positioned at points of unstable equilibrium, then thermodynamic fluctuations will serve as a mechanism for initial grating formation.

Our studies regarding the nonlinear-optical characteristics of these systems for four-wave-mixing processes indicate that translational optomechanical media are a promising class of candidates for both phase conjugation and harmonic phase conjugation at microwave, millimeter wave, and submillimeter wavelengths. The large nonlinear-optical susceptibilities associated with these translational gratings as well as the reasonable response times of these media enhance their potential as active optical media for long-wavelength applications.

[1] P. W. Smith, A. Ashkin, and W. J. Tomlinson, Opt. Lett **6**, 284 (1981).

[2] A. Ashkin, J. M. Dziedzic, and P. W. Smith, Opt. Lett. **7**, 276 (1982).

[3] P. W. Smith, P. J. Malony, and A. Ashkin, Opt. Lett. **7**, 347 (1982).

[4] P. W. Smith, A. Ashkin, J. E. Bjorkholm, and D. J. Eilenberger, Opt. Lett. **10**, 131 (1984).

[5] D. Rogovin and S. Sari, Phys. Rev. A **31**, 2375 (1985).
[6] R. Shih, H. Fetterman, W. Ho, R. McGraw, D. Rogovin, and B. Bobbs, Phys. Rev. Lett. **65**, 579 (1990).
[7] A. J. Palmer, Opt. Commun. **30**, 104 (1979).
[8] A. J. Palmer, Opt. Lett. **5**, 54 (1980).
[9] D. Rogovin and T. P. Shen, IEEE Microwave and Guided Wave Lett. **1**, 388 (1991).
[10] R. McGraw and D. Rogovin, Phys. Rev. A **34**, 689 (1986).
[11] D. Rogovin, R. McGraw, and P. Yeh, Phys. Rev. Lett. **55**, 2864 (1985).
[12] D. Rogovin and T. P. Shen, J. Appl. Phys. **71**, 5281 (1992).
[13] F. Reif, *Fundamentals of Statistical and Thermal Physics* (McGraw-Hill, New York, 1965).

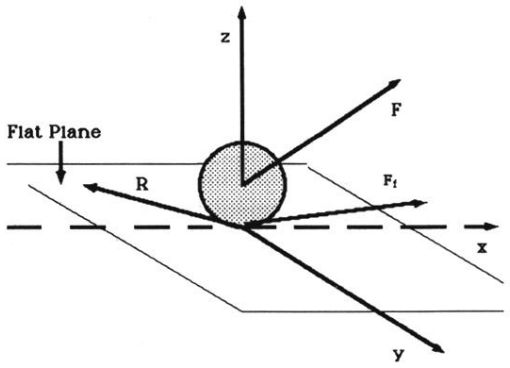

FIG. 2. A sphere rolling on a perfectly rough, flat plane and subject to electrostrictive and frictional forces and torques.